Interplanetary Fast Shocks and Associated Drivers Observed Through the Twenty-Third Solar Minimum by WIND Over Its First 2.5 Years

D. Berdichevsky,* A. Szabo, R. P. Lepping and A. F. Viñas

Laboratory for Extraterrestrial Physics
NASA-Goddard Space Flight Center
Greenbelt, MD 20771

and

F. Mariani

Dipartimento di Fisica
Universita' Tor Vergata
Roma, Italy

Abstract. A list of the interplanetary (IP) shocks observed by WIND from its launch (in November 1994) to May 1997 is presented. Forty two shocks were identified. The magnetohydrodynamic nature of the shocks is investigated, and the associated shock parameters and their uncertainties are accurately computed using a practical scheme which combines two techniques. These techniques are a combination of the "pre-averaged" magnetic-coplanarity, velocity-coplanarity, and the Abraham-Schrauner-mixed methods, on the one hand, and the Viñas and Scudder [1986] technique for solving the non-linear least-squares Rankine- Hugoniot shock equations, on the other. Within acceptable limits these two techniques generally gave the same results, with some exceptions. The reasons for the exceptions are discussed.
It is found that the mean strength and rate of occurrence of the shocks appears to correlated with the solar cycle. Both showed a decrease in 1996 coincident with the time of the lowest ultraviolet solar radiance, indicative of solar minimum and start of solar cycle 23, which began around June 1996. Eighteen shocks appeared to be associated with corotating interaction regions (CIRs). The distribution of their shock normals showed a mean direction peaking in the ecliptic plane and with a longitude (φ_n) in that plane between perpendicular to the Parker spiral and radial from the Sun. When grouped according to the sense of the direction of propagation of the shocks the mean azimuthal (longitude) angle in GSE coordinates was ~ 194° for the fast-forward and ~ 20° for the fast-reverse shocks.

---

*Also, ITSS, Raytheon Corp. Lanham, MD 20706.

Another 16 shocks were determined to be driven by solar transients, including magnetic clouds. These shocks had a broader distribution of normal directions than those of the CIR cases with a mean direction close to the Sun-Earth line. Eight shocks of unknown origin had normal orientation well off the ecliptic plane. No shock propagated with longitude $\varphi_n \geq 220\pm10°$, this would suggest strong hindrance to the propagation of shocks contra a rather tightly winding Parker spiral. Examination of the obliquity angle θ_{Bn} (that between the shock normal and the upstream interplanetary magnetic field) for the full set of shocks revealed that about 58% were quasi-perpendicular, and some were very nearly perpendicular. About 32% of the shocks were oblique, and the rest (only 10%) were quasi-parallel, with one on Dec. 9, 1996 that showed field pulsations. Small uncertainty in the estimated angle θ_{Bn} was obtained for about 10 shocks with magnetosonic Mach numbers between 1 and 2, hopefully significantly contributing to studies researching particle acceleration mechanisms at IP shocks, and to investigations where accurate values of θ_{Bn} are crucial.

1. Introduction

This work was motivated first by the need to provide new and reliable information to the space physics community on properties of the interplanetary (IP) shocks observed by WIND from launch in November 1994 to mid 1997; second, to identify when possible the specific shock drivers, important for multi-spacecraft coordinated observations of the heliospheric region; and third, to provide a physical interpretation of these findings. Finally, we use this opportunity to demonstrate, for this relatively large set of events, the practical value of using some well known, simpler, techniques for fitting shock parameters, as well as the comprehensive technique by Viñas and Scudder [1986; see also Szabo, 1994], and to show how often these techniques provide agreement.

IP shocks are important because they are the source/generation mechanism for energetic particles, and an unusual large number of field and plasma features including turbulence and wave activity near the Sun and in the interplanetary medium (e.g., Gosling and Robson, 1985, and Bougeret, 1985, respectively). Also, as suggested by Gold [1955], some IP shocks may be the precursor to the arrival of large scale heliospheric structures leading to geomagnetic disturbances. This effect, in fact, was later observed to be generally true [Zwickl, et al., 1983; Cane et al., 1987, 1988; Burlaga et al., 1987]. This opened the way to current investigations in the discipline of space weather [Gonzalez, et al., 1989; Reames et al., 1996; Lepping et al., 1997; Burlaga et al., 1981, 1998; Jordanova et al., 1998; Reiner et al., 1998]. For a historical review see Silverman, [1990].

Silverman, [1990]. Hence, it is important to carry out this study using a new set of WIND data providing numerous IP shocks, most of which had not been previously examined.

An IP shock belongs to a family of solar wind discontinuities usually having a thin transition region, representing a surface (as envisioned over some volume) across which there is a flux of matter, and where velocity and magnetic fields vary discontinuously, but mass, momentum and energy is conserved [Landau and Lifshitz, 1960; Tidman and Krall, 1971; Burgess, 1995]. Additionally, an increase in entropy must occur across the shock surface. Under ideal conditions thermodynamic equilibrium occurs on both sides of the IP shock surface, excluding the dissipating transition layer, in which case it is a magnetohydrodynamic (MHD) propagating structure. Whereas the MHD nature of the solar wind fluid allows for the existence of several kinds of MHD discontinuities [Anderson, 1963; Jeffrey and Taniuti, 1964], the IP shocks commonly observed in the heliosphere divide into two general types, namely, fast and slow shocks (Tidman and Krall, 1971; Burlaga, 1995].

Assuming that a shock can be locally well represented by a plane surface (i.e., over a scale-length of tens of R_E), the MHD shock Rankine-Hugoniot (R-H) equations are usually rendered in simple algebraic form [e.g., Tidman and Krall, 1971]. Then, to find the shock normal, **n**, shock velocity, V_S, and θ_{Bn} (i.e., the angle between **n** and the upstream IP magnetic field, IMF), it is necessary only to insert in the equations the properly averaged solar wind conditions for upstream and downstream of the shock. However, it has sometimes been difficult to implement this in practice, using observations of solar wind sampled by only a single spacecraft, because of the non-steady nature of the local solar wind conditions containing fluctuations and discontinuities.

This study uses a fast and reliable method of analysis of the MHD properties of the IP shock. It is a mixture of the traditional pre-averaged methods, i.e., magnetic coplanarity, velocity coplanarity, and mixed Abraham-Schrauner [1972] methods, with the complementary demand that there be a pair of time intervals upstream and downstream of the IP shock where at least two out of the three methods give the same shock parameters (**n**, V_s, and θ_{Bn}). This study shows that this "mixed method" usually constitutes an accurate technique for the determination of the shock parameters.

A determination of the quality of the mixed method is obtained by comparing IP shock parameters results with the corresponding parameter estimations from the powerful and currently most complete non-linear least square R-H fitting method [Viñas and Scudder, 1986; Szabo, 1994]. The combination of both methods in this paper is described as a "working scheme" which

allows the precise determination of shock parameters and their uncertainties. We use it to estimate and evaluate the shock parameters for all MHD fast IP shocks identified by WIND over the period of interest.

The list of shock parameters presented contains most shocks which passed by Earth from the decreasing phase of the 22nd to the start of the rising part of the 23rd solar cycle. During almost all of this time WIND was located in the solar wind upstream of the Earth, where the science operation time of WIND instruments accounted for ~ 97% of its flight time. The apparent association of the observed shocks to their "drivers," when identified is important. Hence, we emphasize this association with regard to the two major types of drivers, i. e, either (1) interfaces of stream-stream interaction regions (corotating interaction regions, CIR's), or (2) solar wind transient interfaces, magnetic clouds being a principal type of such transients [Burlaga, 1995; Gosling et al., 1974].

In section 2 we introduce the working scheme employed and briefly discuss its use to determine the shock parameters and their uncertainties. Shock normals and magnetofluid shock parameters are presented at the end of section 2. Section 3 discusses the shock strength, orientation, association to a driver and other properties in the context of their observations near the start of the 23rd solar cycle, at the solar minimum in 1996. Section 4 focuses on the characteristics of some cases that were difficult to analyze. Summary and conclusions are presented in Section 5.

2. Methods of Analysis

This section describes the data analysis, starting from the identification of an IP shock, through characterization of the data-set employed in the study, and formulation of assumptions about the nature of the shock, to the development of the working scheme used for the analysis of the IP shock properties. For the identification of an MHD IP shock it is necessary to check the mean magnetofluid conditions upstream and downstream of the event against definitions of various known types. For this purpose we reviewed daily WIND summary plots (WIND/ SWE and WIND/MFI) of 92 seconds key parameter data [Mish et al., 1995; Peredo et al., 1996]. We also cross-referenced our identifications with IP shock lists compiled by other workers [viz., by P. Kellog, D. Larson, D. Reames, Z. Smith, private communications 1997].

The data used for these shock studies are: 3 sec averaged IMF data from the magnetic field instrument (MFI) [Lepping et al., 1995], and depending on the solar wind conditions 15 to 21 s snap-shots of the average solar wind ion plasma quantities (proton density, velocity, and temperature) every 46 or 92 s (depending on telemetry mode), and solar wind electron temperatures, all from the solar wind experiment (SWE) [Ogilvie et al., 1995].

Important requirements for the validity of the analysis are that [see Viñas and Scudder, 1986]:

(1) Locally the shock has a simple planar surface, which separates two different states of the plasma, viz., those upstream and downstream, and the shock's motion normal to its surface defines a Galilean frame of reference (i.e. it is not accelerating).

(2) The considered data points mix in a statistical way which cancels the contributions from the plasma turbulence present in the analyzed intervals. These requirements are equivalent to the demand that the R-H conservation equations [see, e.g., Burlaga, 1995] hold true for the intervals under consideration. These equations are:

$$\Delta [\rho(\mathbf{V} \cdot \mathbf{n} - V_S)] = 0 \quad (1)$$

$$\Delta[\mathbf{B} \cdot \mathbf{n}] = 0 \quad (2)$$

$$\Delta[\mathbf{V} \times \mathbf{B}] = 0 \quad (3)$$

$$\Delta [\rho (\mathbf{V} \cdot \mathbf{n} - V_S)\mathbf{V}_t - B_n/\mu_O \mathbf{B}_t] = 0 \quad (4)$$

$$\Delta [(\mathbf{n} \times \mathbf{V}_t) \mathbf{B}_n - (\mathbf{V} \cdot \mathbf{n} - V_S) (\mathbf{n} \times \mathbf{B}_t)] = 0, \quad (5)$$

where Δ followed by square brackets indicates the difference between the upstream and downstream mean values of the enclosed observables. In these equations, **V** is the "bulk" velocity of the solar wind, ρ is the mass density of the solar wind ions, and **B** is the IMF. The subscripts n and t indicate the normal and tangential directions with respect to the shock plane, and V_S is the speed of the shock relative to the upstream plasma defined to be along the unit shock normal **n**.

General conventions and rules for the analysis of the IP shocks follows. With respectively identify with "up" the value of any parameter upstream the shock and with "dw" its value downstream. The direction of propagation of the IP shock is defined to be along its surface normal with a sense opposite to the direction matter flows relative to the shock surface. The IMF and plasma data are restricted to the SW conditions in intervals no larger than two hours, before and after the time of the shock transition (or ramp). For this purpose ~ 15 second solar wind H^+ averages, spaced every 46 or 92 s, are combined with the value of 3 second average IMF data, averaged to the same resolution and instant as the plasma data. The resulting data set is used in the determination of the orientation of the MHD IP shocks normal **n**, speed V_s and the angle θ_{Bn}, between **n** and the upstream IMF. Other general rules used in the analysis are: (a) the chosen upstream and downstream intervals do not overlap the shock discontinuity (its ramp) and are sufficiently far apart to avoid the inclusion of non-MHD kinetic structures, (b) the intervals are

as close to the shock as is necessary for their plasma/field states to be valid for use in Equation 2, i.e., not be distorted by any convective structures in the vicinity of the shock. Uncertainties in the determination of the shock parameters result from the compromise between these two conditions. Additional guides in our search for the best possible solution are the requirements that the shock be supermagnetosonic and entropy increases across its surface.

The working scheme can be briefly summarized as a two-step method. In a first step we take advantage of the use of the fast pre-averaged (p-ave) methods for the evaluation of the shock parameters and their errors as a function of a set of chosen upstream and downstream regions of the shock. This is presented in subsection 2.1. In a second step we choose the optimal pairs of upstream and downstream time intervals found in step one, to solve for the shock parameters which satisfy the R-H equations; i.e. we perform a non-linear least square R-H fit to the data to obtain the self-consistent solution within the available experimental accuracy. This is presented in subsection 2.2.

Because of the R-H ansatz none of these methods, presented in subsections 2.1 and 2.2, allow for a dynamically evolving shock structure over the time that the spacecraft passes from one side to the other, including the time considered in the full pre- and post-shock state. That is, if the IP shock is non-stationary, our fit methods break down. This is indicated above under "requirement no. 2." The implications of this limitation will be discussed in Section 4 using some specific examples.

2.1. The p-ave Technique

This section shows how the pre-averaged (p-ave) methods are used to obtain accurate determinations of the MHD shock parameters for most fast IP shocks. The p-ave methods were extensively investigated by Abraham-Shrauner [Abraham-Shrauner, 1972; Abraham- Schrauner and Yun, 1976] with the following results:

(a) Magnetic-coplanarity (mc) takes advantage of one of Maxwell's equations, $\nabla \bullet \mathbf{B} = 0$, which is essentially R-H Equation (2), which in principle provides an unambiguous determination of the shock normal, but it has two common problems. One is the sensitive dependence of the method on the fluctuations/discontinuities of the IMF which become nearly comparable to the value of the mean field for near parallel shocks. The other problem is that the method fails for perpendicular shocks and gives very poor results for near-perpendicular shocks. In the latter case the IMF upstream and downstream of the shock become nearly parallel to each other with a negligible **B** component in the shock normal direction, causing the orientation of the plane of the shock to become undetermined.

(b) Velocity-coplanarity (vc) is exactly valid for pure parallel and perpendicular shocks [see R-H Equations (3) and (4)]. But it is only approximately valid for quasi-perpendicular shocks and the solution is unstable for near parallel shocks.

(c) The Abraham-Shrauner (AS) mixed method corrects the problem of the undetermined normal for near perpendicular shocks which occurs with the mc method. It also decreases the uncertainties resulting from the vc method, which in most cases can give only an approximate solution. The inaccuracies of the method can usually be traced to the difficulty in correctly choosing the upstream and downstream mean MHD analysis-intervals, which provide self consistent parameter pairs across the shock.

We find that our p-ave technique is accurate in determining the shock normal, and consequently the shock parameters, by demanding that good MHD parameter pairs (up- and down-stream) across the shock (i. e., for ρ, **V** and **B**) give the same shock normal for at least two of the three methods discussed above. We do not demand that the three methods always agree, because neither the mc nor the vc methods are valid for the full range of orientations of the IP shock normal relative to the IMF.

The following four statements outline the practical scheme for determining the shock parameters using the p-ave technique:

i) After selecting the upstream and downstream analysis-intervals for the shock we take the average of the IMF and plasma moments for these intervals; hence, its name "pre-averaged technique" (p-ave).

ii) For these parameter pairs we calculate the shock normal direction using the mc, vc, and AS methods (see Appendix A), and then check to see that the normals calculated from at least two of the three different methods agree within 15°, an angle based on our experience with past studies of IP shocks and on the reasonableness of such tolerance; this represents a 1-s.d. uncertainty.

iii) We check to see if the direction of the velocity of the shock (determined by using R-H Equation (1)) is compatible with the nature of the shock (i.e., forward, F, or reverse, R, IP shock), and if the shock-speed upstream is supermagnetosonic (i.e. having a shock speed large than $(V_{Alfvèn}^2 + V_{Sound}^2)^{1/2}$); when the latter condition is satisfied, the shock will be superalfvènic and supersonic. The plasma Alfvènic and shock magnetosonic Mach numbers are also presented here.

iv) Finally, we check to see that the solution shows only small violations of the R-H conditions from Equations (3) to (5), i.e.,

$$2\Delta[Q]/(|Q_{up}| + |Q_{dn}|) << 1, \qquad (6)$$

with [Q] representing any of the quantities in the R-H equations, and we also check to see that there is an entropy increase in going from the upstream to the downstream region. (For determinations of the direction of entropy change and the fast mode magnetosonic Mach number of the shock we use the mean value of the electron and proton temperatures for a time interval of nearly one hour before and after the shock).

The mean value of the estimated normals becomes our first solution to the problem. If the normals do not coincide within ~ 15°, new time intervals are tried until an acceptable solution is found, i.e., one which gives approximately the same normal directions to the shock for at least two methods. Otherwise, the indication is that the determination has either been obtained with the help of other information (e.g., the speed of propagation of a transient following the shock), it is of poor quality, or the method failed to give a solution.

A shock solution consistent with conditions (ii) and (iii) will constrain the upstream and downstream analysis intervals, and therefore the averages of **B**, ρ, and the solar wind **V**-field quantities. These are then considered to be the equilibrium values upstream and downstream of the shock. Hence, the resulting normal **n** should be the most likely solution for the shock. We explicitly check condition (iv) (i.e., shock solutions must cause only small violations of the R-H Equations (2) to (5)), and we use Equation (1) to estimate the shock velocity, as has been done customarily in the past [Lepping and Argentiero, 1971 and Viñas and Scudder, 1986]. Once the IP shock solution is found we proceed to study the uncertainty and stability of the estimated shock normal, **n**, and the upstream orientation of the magnetic field, $\mathbf{B}_{up}$, against small variations of the selected up- and down-stream analysis-intervals. Three examples of this (April 7 and June 26, 1995, and June 18, 1996) are illustrated by the histograms in Figure 1 for various analysis-intervals, which show related distributions of shock normals. In this way we can generate an ensemble of solutions $\{\mathbf{n}\}$, and $\{\mathbf{B}_{up}\}$. We can then calculate the mean and standard deviation of the shock normals and the acute angles θ_{Bn} for each case. In doing so we weigh each solution, i.e., the pairs of angles (θ_n,φ_n) and (θ_B, φ_B), which respectively define the orientation of the shock normal and the direction of $\mathbf{B}_{up}$, as described below.

The vc solutions are weighted with the geometric mean of the absolute values of $1/(\mathbf{t} \bullet \mathbf{n}_{vc})$ and $1/(\mathbf{s} \bullet \mathbf{n}_{vc})$, with **t** and **s** given by

$$\mathbf{t} = (\mathbf{B}_{up} - \mathbf{B}_{dw})/|\mathbf{B}_{up} - \mathbf{B}_{dw}|, \quad (7)$$

the direction tangent to the shock, and

$$\mathbf{s} = (\mathbf{B}_{up} \times \mathbf{B}_{dw})/|\mathbf{B}_{up} \times \mathbf{B}_{dw}|, \quad (8)$$

the direction perpendicular to the coplanarity plane (containing **n** and **t**), and where up and dw mean up- and down-stream, respectively. We believe that this is a good way of weighting the quality of the solution to the normal given by the vc recipe (Appendix A), because although $\mathbf{s} \bullet \mathbf{t} = \mathbf{s} \bullet \mathbf{n} \equiv 0$ are required mathematically, actual solutions to $\mathbf{n}_{vc}$ are by definition approximate solutions in most cases. When this is coupled to data and mathematical uncertainties of the evaluation, small but non-zero values for $\mathbf{t} \bullet \mathbf{n}_{vc}$ and $\mathbf{s} \bullet \mathbf{n}_{vc}$ are almost certainly assured, and the smaller their values the larger our weighting factor for the solution. (In fact, after hundreds of trials performed in this study, across all the various shocks, we did not encounter the limiting situation of $\mathbf{s} \bullet \mathbf{t} = \mathbf{s} \bullet \mathbf{n} \equiv 0$.) The normal $\mathbf{n}_{vc}$ is that derived from the velocity coplanarity technique (vc). In a similar fashion the AS weighting factor is the absolute value of $1/(\mathbf{s} \bullet \mathbf{n}_{AS})$. Here, no dependence on $\mathbf{t} \bullet \mathbf{n}_{AS}$ is included, because the AS coplanarity solution imposes $\mathbf{t} \bullet \mathbf{n}_{AS} \equiv 0$. For the mc solutions ($\mathbf{n}_{mc}$) the weighting factor used is 1.0. This follows from the definition of the mc technique, which imposes $\mathbf{t} \bullet \mathbf{n}_{mc} \equiv \mathbf{s} \bullet \mathbf{n}_{mc} \equiv 0$. In this way the mean normal and standard deviation generated by the average-method technique, using an ensemble of shock normals, will give a solution consistent with the following constraints:

$$B_n(up) - B_n(dw) = 0 \quad (9)$$

$$B_s^2(up) + B_s^2(dw) = 0 \quad (10)$$

and

$$|V_s(up)| - |V_s(dw)| \equiv 0, \quad (11)$$

making this technique equivalent to the one introduced by Whang et al. [1996].

The shock parameters resulting from the p-averaged technique are listed in Table 1. These include the following:

On the left side of the table we present, from columns 1 to 5, the shock identification number, year, date and time of the shock, and time intervals up- and down-stream of the shock. On the right side, columns 6 to 15 present, with their standard deviation (± s.d.), the shock normal orientation in GSE coordinates (longitude φ_n and latitude θ_n), the shock velocity V_S relative to the

solar wind, the shock type (forward = F or reverse = R), the mean value of the IMF vector B_{up} (upstream of the shock in GSE coordinates), the angle between the shock normal and B_{up} (θ_{Bn}) and the average method used (vc, mc, and/or AS) which provides normals that agree within 15°.

2.2 The Non-Linear Least Square (R-H) Technique

Currently the most comprehensive methods of MHD shock fitting to the R-H equations are the similar non-linear least square fitting techniques (R-H) of Viñas and Scudder [1986] and Szabo [1994]. The latter makes use of the normal momentum and energy flux conservation equations beside the other R-H equations, and it adds the calculation of the confidence regions for the solutions. These techniques have the advantage that they do not require the pre-determination of the average MHD values of the magnetofluid parameters upstream and downstream of the shock, unlike the pre-averaged methods detailed above. The only noteworthy limitation of these methods is that the analysis-intervals appropriate for MHD considerations have to be manually set. But within these upstream and downstream windows all measured data points are included, and as part of the fitting process not only the best-fit shock normal and shock propagation speed is determined, but also the asymptotic magnetofluid parameters on both sides of the shock that are constrained to be self-consistent with the MHD equations and consequently are the best-fit values possible for the observations. Therefore, plotting the calculated asymptotic values on top of the observations reveals the quality of the fit; or alternatively the reduced χ^2 fit parameter indicates the goodness of the fit. See Figure 2 which shows asymptotic values (as horizontal lines, with gray-shaded 1standard deviations (s.d. or σ)) for the various plasma and field quantities for the cases that were discussed earlier in terms of the p-ave technique: June 26, 1995 (RQperp), and June 18, 1996 (FQperp). A more quantitative measure of the goodness of the fit is given by Szabo [1994], where the individual measurement uncertainties coupled with the fitting discrepancies are carried through all calculations, and proper confidence regions around the solutions are obtained, with the only assumption being that the observational uncertainties are assumed to have a Gaussian distribution. Visualizations of the uncertainty regions are shown in Figure 3, indicating the quality of the shock normal determination. When the shock normal is determined to a high degree the uncertainty regions are tight small regions around the best fit direction (Figure 3a). Lower quality fits (like Figure 3b), however, are not without value. In the case of the 1996 June 18 shock, most uncertainty lies in one particular direction and the shock is resolved quite well in the other. This illustrates the power of the R-H method, namely that even for more complex situations, where the other methods tend to fail, significant amount of information can be recovered.

In our study the one sigma (68%) confidence levels are used as error bars to compare the R-H

best-fit results with those of the p-ave methods. We also address the question of uniqueness of the solutions. With the R-H method we successfully decouple the 11- dimensional fitting parameter space into no more than 2-dimensional sub-problems which can be graphically mapped, and all likely solutions investigated. Most of the IP shocks encountered in this study have a unique solution. However, a few have a number of equally likely but different solutions (usually indicating poor quality fits). These will be discussed separately in Section 4.

2.3. Quality of the Shock Normal and θ_{Bn} Estimates

Both methods show overall agreement in the resulting shock-normals, as illustrated in Figures 4. With the p-ave technique we explored the uncertainty to the normals associated with different time intervals. The R-H technique searches for a R-H solution of the shock normal (i.e., to Equations 1-5) and its uncertainty, among other quantities, for the most likely set of upstream and downstream analysis-intervals. It is then apparent that the actual uncertainty in the normal corresponds to the addition of the derived errors from the p-ave and R-H methods. We consider our determination of the shock normal to be accurate when the solutions using the p-ave and R-H techniques agree within the overall error uncertainty. The sum of the scalar product of the shock normal and its uncertainty

$$\mathbf{n}_{p\text{-}ave} \bullet \mathbf{n}_{R\text{-}H} + \Delta(\mathbf{n}_{p\text{-}ave} \bullet \mathbf{n}_{R\text{-}H}) \quad , \tag{12}$$

where

$$\mathbf{n}_{p\text{-}ave} \bullet \mathbf{n}_{R\text{-}H} = \cos(\varphi_{p\text{-}ave})\cos(\theta_{p\text{-}ave})\cos(\varphi_{R\text{-}H})\cos(\theta_{R\text{-}H}) + \sin(\varphi_{p\text{-}ave})\cos(\theta_{p\text{-}ave})\sin(\varphi_{R\text{-}H})\cos(\theta_{R\text{-}H}) + \sin(\theta_{p\text{-}ave})\sin(\theta_{R\text{-}H})$$

and

$$\Delta(\mathbf{n}_{p\text{-}ave} \bullet \mathbf{n}_{R\text{-}H}) = \sin(\varphi_{p\text{-}ave}-\varphi_{R\text{-}H})\cos(\theta_{p\text{-}ave})\cos(\theta_{R\text{-}H})(2\Delta\varphi) + \sin(\theta_{p\text{-}ave}+\theta_{R\text{-}H})\,[1+\cos(\varphi_{p\text{-}ave}-\varphi_{R\text{-}H})]\,\Delta\theta,$$

(with $\Delta\theta = \Delta\theta_{p\text{-}ave} \approx \Delta\theta_{R\text{-}H}$ and $\Delta\varphi = \Delta\varphi_{p\text{-}ave} \approx \Delta\varphi_{R\text{-}H}$) is a single number indicative of the agreement or disagreement between the p-ave and R-H shock normals. This quantity is unity for $\mathbf{n}_{p\text{-}ave} = \mathbf{n}_{R\text{-}H}$ for negligible uncertainties. A value larger or equal to 1.0 in Relation (12) is then interpreted as indicative of agreement within the uncertainties associated with the measurement and analysis. A value smaller than 1.0 in Relation (12) is interpreted as a case of disagreement between the p-ave normal $\mathbf{n}_{p\text{-}ave}$ and the R-H normal $\mathbf{n}_{R\text{-}H}$. (The test of the shock normals, using Relation 12, shows satisfactory agreement for most cases; see Figure 5.) Disagreements in the shock normals are essentially limited to the shocks discussed in Section 4.

Historically, the angle θ_{Bn} (i.e., the absolute value of $\cos^{-1}(\mathbf{n} \bullet \mathbf{B}_{up}/B_{up})$), has been used as the

basis of classification of shocks into quasi-perpendicular, oblique, and quasi-parallel categories, which are known to correspond to different upstream and downstream plasma characteristics, as well as markedly different kinetic profiles. (This was based on experience gained primarily from the study of the Earth's bow shock.) Uncertainties ($\Delta\theta_{Bn}$) in the value of θ_{Bn} are the result of uncertainties in the shock normal and the MHD value (i.e., effective steady-state value) of the IMF upstream of the shock. Therefore, the uncertainties $\Delta\theta_{Bn}$ are larger than the uncertainties in only the orientation of the shock normal. A shock's magnetosonic Mach number and its character depend markedly on θ_{Bn} and the upstream shock velocity [Tidman and Krall, 1971]. Our evaluation of the uncertainties in θ_{Bn} are discussed in Appendix B.

3. Results

Table 2 presents: the sense of shock propagation (i.e., F or R), an estimate the orientation of the shock normal, its speed with respect to the upstream solar wind, and the angle θ_{Bn} for each of the WIND shocks, covering the period from November 20, 1994 to May 31, 1997. These quantities are based on a combination of the results of the various averaging methods (mc, vc, and AS in the context of our p-ave scheme) and the R-H technique.

The statistical synthesis of the R-H shock parameters in this study is presented in Table 3 in terms of the mean values and standard deviations (s.d.) of the estimated shock velocity, magnetosonic Mach number (M_S), shock normal longitude (φ_n) and latitude (θ_n), and the shock obliquity (θ_{Bn}) relative to the upstream IP magnetic field. The mean shock velocities for F or R IP shocks in GSE coordinates are ~ -320 ± 90 and -670 ± 100 km/s, respectively, based on the immediate upstream solar wind speed. Table 3 shows that on average the fastest shocks were the R ones, and the slowest were the ones without a known driver. The latest ones were also the weakest. The largest spread in the distribution of M_S occurred for the transient driven shocks, although a comparable spread occurs for the R shocks. The mean orientation of the IP shocks was along the Sun-Earth direction with a spread between 20° and 30° depending on the type of shock considered. The shocks with unknown drivers have the largest deviations relative to the plane of the ecliptic. Table 3 shows that the average obliquity ($<\theta_{Bn}>$) of all shocks is close to 60° with a standard deviation of 25°. Table 3 also shows that the shocks without known drivers were the more quasi-perpendicular ones with a $<\theta_{Bn}>$ ~ 72° and a standard deviation of ~ 15°.

3.1 Frequency, strength, and drivers of IP shocks: Dependence on the solar cycle

Over the 2-1/2 years of interest we identified 34 forward and 8 reverse fast IP shocks. It is interesting that during 1996, when the minimum in the 11 year solar cycle occurs [Ogawa et al., 1998] the lowest frequency in shocks occurred (see Figure 4). When classified by their velocity, Figure 6a shows 14 or 15 shocks with $V_s > 100$ km/s, and a slower group with a mean speed of ~ 60 km/s (see Table 2). Possibly a more valid classification is by magnetosonic Mach number, M_S By such a classification the shocks appear to divide again into two groups. One group, which we call "weak" shocks, has M_S values smaller or equal to 1.3 (i.e. having shock velocities 30% larger than the fast mode wave speed.) The group of shocks with M_S values greater than or equal to 1.5 contains one event with a shock velocity nearly 2.5 times the fast magnetosonic wave velocity. We call the 17 shocks belonging to this group "strong". They have a mean M_S ~ 1.8. Figure 6b illustrates the dependence of the strength of the IP shocks on time. Notice that during the whole year 1996 (i.e., minimum in the solar cycle) only one shock meets our "strong" shock criterion. Table 4 organizes the shocks by their magnetosonic Mach number in two sets, in Table 4a those with a magnetosonic Mach number ≥ 1.5 and in Table 4b those with a magnetosonic Mach number < 1.5. Tables 4a and 4b also present the value of the shock velocity in Earth's frame of reference, the ratio of the shock speed (solar wind frame) to the alfvènic speed and in the last column the possible driver associated to the shock,

There are different types of IP shock drivers. Interplanetary coronal mass ejections (IP-CME's or ICME's)/magnetic clouds are good examples of transient drivers. Stream- stream interfaces or corotating interactive regions (CIR's) are quasi-periodic shock drivers; see e.g. Gosling et al., [1972], Gosling, [1981], Burlaga, [1974, 1995]. However, it has been argued that CIR's seldom develop shocks within 1 AU [Pizzo, 1981; Smith and Dryer, 1991, and references therein]. An estimate of the percentage of IP shocks observed at 1 AU associated with CIR's may help test the predictive power of current MHD IP shock models discussing CIR's [Steinolfson, et al., 1975; Smith and Dryer, 1991]. On the other hand, the results presented here for shocks associated with ICME could be used to test the MHD modeling of IP shocks, depending on initial conditions associated with a solar transient event [Dryer, 1994; Lario, 1997]. A hypothetical so-called blast wave shock, apparently having no driver and therefore probably born and set in motion at the Sun, cannot be easily distinguished (with a single spacecraft's measurements) from a shock having a driver that is simply not seen by the spacecraft. And this can easily happen if the shock's driver is sufficiently "off to the side," with respect to the spacecraft's position which may occur for some cases where the driver subtends a narrower angle than its shock (**Cane et al., 1988; Reames et al., 1996**).

The locally occurring solar wind IMF and plasma conditions naturally influence the correct

identification of a driver of an IP shock. In the case of a magnetic cloud (or cloud-like ejecta) the overall profile of the interaction-features observed, in time order, are: the upstream IP shock, a sheath region of many hours (but usually distinctly less than a day), an occasionally well-defined front boundary of the cloud, the strong sustained field region of the cloud itself (i.e., with respect to the upstream IMF), and a rear boundary. The cloud's front boundary, the likely immediate driver surface of the shock, may be a tangential discontinuity. Within the cloud the proton temperature is markedly lower than its upstream value [Burlaga, 1995]. These overall properties were used to identify such a transient region in this study.

Between the launch of WIND (11/1994) and mid 1997 the WIND observations cover solar conditions extending from the end of solar cycle 22 to the beginning of the solar cycle 23 (which we take as solar minimum); see, e.g., Ogawa et al., [1998]. Sanderson et al. [1998] illustrate the main characteristics of the solar wind during this period. Panels d-f of their composite Figure 2 indicate approximately 120 main IMF polarity changes at the location of WIND. Most of these crossings were associated with regions of compressed field and plasma. They consistently matched, in time, observations at WIND of a streamer belt solar wind being deflected by a high speed stream coming from solar coronal hole(s). The coronal holes in 1994 and until 1996 extended from the Sun's pole to quite low latitudes, usually making possible related observations of nearly pure high speed streams at low latitudes at 1 AU. It was possible to relate fast strong F (one) and R (five) IP shocks to this time interval (see Table 4a). Other strong shocks related to CIRs occurred on Sept. 1996, and Jan. and March 1997. Table 4b shows other (9) weaker shocks likely to be related to CIRs. Only one pair of F and R IP shocks related to CIR's was identified. These two shocks occurred on Dec. 24 and 25, 1995 respectively. Of the four strong fast F IP shocks that were observed to be driven by magnetic clouds (transient example) in this period [Lepping et al., 1999], two of them (one on Oct 1995 [Lepping et al., 1997] and the other on Jan. 10, 1997 [Burlaga et al., 1998]) were followed by high-speed streams suggesting the possibility of an association between the transients (clouds) and the CIRs. These two magnetic clouds may have originated near coronal holes [see e.g. Watari and Watanabe, 1998]. From these we get a total of 18 IP shocks associated with CIRs and 2 strong forward IP shocks associated with magnetic clouds being overtaken by fast streams, and a total of four strong fast F IP shocks driven by magnetic clouds, including the two compound cases. These compound cases could be those of magnetic clouds becoming part of a CIR structure. Our results shows that at 1 AU low latitude CIR shocks formed in at least 15% of the cases, and often they were strong R shocks. But also some F shocks were driven by CIR's, and all of them appear to be associated with coronal holes that extended to nearly the Sun's equatorial latitude.

Three other strong F IP shocks were also associated with solar transients ("t" in Table 4a). The first one is the F IP shock on Oct. 22, 1995. It is associated with a strong west limb CME which

also produced a high intensity flux of energetic particles at Earth. This shock associated event started at 0655 UT on Oct 20, 1995 at the Sun [Reames et al., 1997]. Gopalswamy et al., [1998b] investigated the solar origin of the driver of the Feb. 9, 1997 forward IP shock, which, in this study, is the fastest moving shock relative to Earth. The IP shock of April 10, 1997 appears to be the lateral northward extent of a F IP shock driven by a fast CME (~ 800 km/s), from observations with the LASCO/SOHO coronagraph [Berdichevsky et al., 1998]. Two other strong IP shocks also appear to be driven by transients of solar origin ("t?" in Table 4a). There are two weak F IP shocks, one on Aug 22, 1995 and the other on May 26, 1997 that are associated with solar transients. There may be three more candidates (t? in Table 4b). One of them, the IP shock of Apr. 11, 1997 is the only R shock in this study that appears associated with a transient [Berdichevsky et al., 1998]. Finally, there are 8 weak IP shocks that we were not able to associate with a driver. For the period before June 1996 there appears to be no association between shocks observed via Type II radio bursts in the lower corona and those observed in situ by WIND in the interplanetary medium [Gopalswamy et al., 1998a]. One of the shocks of unknown origin occurred inside a magnetic cloud (F IP shock on Oct. 19, 1995 [Lepping et al., 1997]).

3.2 On the statistical orientation of normals in the ecliptic plane

Figure 7 sketches the observed mean orientation of F and R shocks. All R shocks, except one, are clearly associated with CIRs. In Figures 8a and 8b we present the distribution in the ecliptic plane of all F and R shocks. The distribution of F shocks shows a concentration in their longitude angle from 180° to 225°. This indicates an orientation between radial from the Sun and the one that would be expected to be normal to a Parker spiral angle at 1 AU (Figure 8a) [see, e.g., Acuña and Whang, 1976; Cravens, 1997]. This distribution of orientations of F shocks projected in the plane of the ecliptic strongly broadens toward smaller angles. This is obviously not a normal distribution in the longitude angle φ_{GSE}. It is, in fact, reminiscent of a Poisson distribution, so we do a least square fit of such a distribution to the data and find quantitively the likely limit angle $\Phi_{GSE} = \varphi_{GSE} = 220 \pm 10°$ beyond which the direction-component on the ecliptic plane of the F shocks appear to be forbidden, at 1 AU. Our best-fitted Poisson distribution to the longitude distribution of shocks then is

$$F(r(\Phi_{GSE}),\lambda) = \lambda^r/\Gamma(r+1)\, e^{-\lambda}, \qquad (13)$$

with a characteristic parameter $\lambda = 1.55 \pm 0.20$, and $r = 2(\Phi_{GSE} - \varphi_{GSE})/45°$, for a number of 31 F IP shocks. Consequently it appears that westward moving F shocks with a larger obliquity than

Φ_{GSE} either decayed before reaching 1 AU or were deflected toward $\varphi_{GSE} < \Phi_{GSE}$. For a much more limited number of R shocks Figure 8b indicates again a clustering between slight departure from the Sun-Earth line and normal to the Parker spiral, which would be expected for well developed shocks associated with CIRs [Hundhausen, 1995; Dryer, 1994]. The distribution in latitude of all fast shocks is also broad, as it is indicated in Figure 8c, with an expected mean value close to the plane of the ecliptic.

It is worth asking if a specific shock normal orientation is uniquely indicative of the nature of the shock's solar wind driver [e.g., Cane et al. 1988; Richardson and Cane, 1993; Reames et al. 1996; Gopalswamy et al., 1998]? A unique relationship is not likely, if only because each type of driver will provide shocks with a relatively broad range of normal orientations depending on the angular displacement between the source and observer, and this broadness is exacerbated by any (and commonly occurring) upstream solar wind variations that cause natural orientation responses in the normal. However, an apparent discriminating relationship, via a bimodal clustering of the normals according to the shock's type of driver, appears to exist statistically during solar minimum (see Figure 9). The fast F and R IP shocks driven by CIR's tend to cluster between a direction radial from the Sun and the one defined by the Parker spiral angle [Cravens, 1997; Acuña and Whang, 1976]. Their distribution of latitudinal orientations shows a strong peak near the Ecliptic plane (Figure 9a). The only R IP shock possibly driven by a transient present in the Ecliptic plane has an orientation close to the Parker spiral angle. All the other driven IP shocks were F shocks, and their distribution appears to peak for directions along the Sun-Earth line (Figure 9b). The distribution in orientations is, however, broader than that for the shocks driven by CIRs. This broader distribution in azimuth (φ_n) and latitude (θ_n) could suggest a larger (average) shock surface curvature, i.e., a smaller spatial extension on average, for shocks driven by ejecta than those driven by CIRs during the current solar minimum.

Finally, the distribution of shocks of unknown origin appear to show orientations pointing well out of the Ecliptic plane, and the small azimuth angles in two of them could suggest an unobserved transient sources (see Figure 9c). The other F IP shocks of unknown origin show directions that could well be consistent with unobserved drivers. These drivers could be either CIRs or ICMEs (ejecta).

3.3 The orientation of the IP shocks relative to the magnetic field

The relative orientation of the shock normal to the IP magnetic field θ_{Bn} is of great importance for many studies in space physics. For example, the study of particle acceleration at shocks indicates that the acceleration of seed and nearly supra-thermal SW particles may depend on the

angle θ_{Bn} and its magnetosonic Mach number M_S [see e.g. Ellison et al., 1995]; see Table 2 (θ_{Bn}) and Table 4 (M_S). Table 2 shows that there was a large number of quasi-perpendicular shocks in our set, 58%. Several of these shocks had an orientation very nearly perpendicular to the IP magnetic field, but there was a much smaller number of IP shocks with a solution for θ_{Bn} close to 0°, namely 10% (see the histogram in Figure 10). The rest were oblique cases, 32%. (In most cases we catalog shocks with θ_{Bn} between 35° and 55° as oblique, and those outside this range as either quasi-perpendicular (for higher θ_{Bn}) or quasi-parallel (lower θ_{Bn}).) However, a final characterization in the assignment of a shock as quasi-perpendicular or quasi-parallel is not only based on the evaluated obliquity of the normal but also after a careful weighting of the overall IMF and plasma conditions at the shock. This is because for example for quasi-parallel shocks the average field from upstream to downstream, for example, is not expected to have any change, in principle; The other plasma quantities (temperature, velocity and density) do change across a parallel shock, of course, as well as the field fluctuation level, which makes such shocks possible to identify. (An example is the Dec 9, 1996 shock in Figure 11.)

A graphical representation, in Figure 10b, of the θ_{Bn} angle versus M_s (which is the other shock parameter relevant to theoretical studies on particle acceleration at shocks [see, e.g., Ellison et al., 1995]) shows that about 12 shocks had small uncertainties in θ_{Bn}. These are shocks with standard deviations in θ_{Bn} (s.d.$\{\theta_{Bn}\}$) << 15°. Another 13 shocks had uncertainties where 15° << s.d.$\{\theta_{Bn}\}$ << 30°, and the remaining 13 shocks had uncertainties (s.d.$\{\theta_{Bn}\}$) larger than 30°. The well determined cases may enable further study of acceleration processes for shocks with 1 < M_s < 2.8.

4. Shocks difficult to fit

In spite of the robust nature of the R-H method and its capability to analyze complex data sets, a number of conditions can severely limit the usefulness of the obtained results. These conditions usually invalidate one of the underlying fundamental assumptions of the fitting procedure, such as severe violation of MHD requirements which occur for example when the fluctuations in magnetic field are comparable to its change due to the shock, i.e., when $\delta B/\Delta[B] \sim \theta_B$ or ϕ_B. Such is the case with the Jan. 1, 1995, and Oct 18, 1995 shocks. Also, if the interplanetary shock is propagating through a rapidly changing region, the change in the ambient field and plasma due to interplanetary discontinuities are hard to separate from the shock induced variations. In such a case the obtained shock normals are of very poor quality (e.g. May 26, 1997). Sometimes, the difficulties associated with solar wind variations are compounded with the presence of

particularly weak magnetic fields, so that the amplitude of variation over the stable MHD values is larger than the asymptotic values. The resulting error bars are unusually large (e.g. Oct. 18, 1995).

Besides difficulties associated with fluctuating solar wind backgrounds, some weak and/or parallel shocks are difficult to fit in their own right. Some particularly weak shocks might be at the very boundary of shocks and pressure pulses, and are notoriously difficult to fit. Such is the case with the unusual shock observed within a magnetic cloud on Oct 19, 1995. The situation is worse when the weak shock is quasi-parallel as this kind of shock is associated with strong wave activity making the identification of upstream and downstream MHD magnetofluid parameter difficult (e.g. Dec. 9, 1996). Some of the weak shock fittings result in multiple, equally likely solutions due to the large uncertainties. When no physical principal can be applied to rule one or the other solutions out, the ambiguity remains (e.g. Dec. 25, 1995, and Jan. 28, 1997).

A final difficulty is posed by the presence of another MHD discontinuity nearby the shock. Due to the different propagation speeds of the various MHD discontinuities, it is inevitable that they interact in the interplanetary medium. Even though the probability to observe such an interaction is rather low, a number of cases have been observed where a discontinuity (usually a tangential one) was within the analysis interval of the shock. When the entities are too close to each other to obtain reliable undisturbed measurements in-between the shock fitting procedure is brought into question. Such was the case for the shocks on Sept. 26, 1996, Dec. 9, 1996, Feb. 9, 1997, and May 20, 1997. These unusual encounters will require a separate and more detailed study. Figure 11 illustrates these conditions for the Dec. 9, 1996 shock, where a tangential discontinuity was observed at ~18:48:10, just two minutes before the observation of the shock clearly delineated by the lower resolution plasma data. The large amplitude pulsations in the IMF observations clearly indicate a relatively weak quasi-parallel. The R-H fitting technique results in a quasi-perpendicular solution but only because of the effect of the shock and the nearby TD cannot be separated in the analysis of the plasma data.

5. Summary and Conclusions

This paper presents the first summary of the results of IP shock analyses based on solar wind data from the SWE and MFI instruments on the WIND spacecraft for the period from launch to May 31, 1997. A comprehensive dual-technique scheme, representing a new analytical philosophy, was developed which allowed us to make reliable shock parameter determinations and associated quality checks. The output parameters include shock surface normals, shock speeds, M_S, θ_{Bn}, and other relevant magnetohydrodynamic quantities; these are presented in Tables 1, 2 and 4.

A by-product of the investigation is the finding, after various comparisons, that a judicious use of the traditional "parameter averaging methods" (part of the dual technique scheme) can be used with a high degree of confidence in most cases. To achieve that confidence, however, it is necessary to carefully choose the right time intervals up- and down-stream of the IP shock. This is achieved by trial, sometimes after many trials. For the right set of such time intervals at least two of the three average methods mc, vc, and AS were required to provide consistent shock surface normals within a small error cone angle (i.e., ~ 15° or less). In using these techniques we set this constraint, and also checked that there were only small violations of the R-H conditions (Equations 1 to 5). We also used the comprehensive method by Viñas, Scudder and Szabo (the other part of the dual technique scheme). This second method determines the asymptotic shock parameters through a non-linear solution of the R-H equations. This method has the advantage over the pre-averaged methods of being less dependent on the choice of the initial selection of the up- and down-stream intervals, because of the important interplay of the field and plasma quantities through the constraining equations. We evaluated the shock normals independently with the "averaging" and R-H techniques, and later compared the results for each shock. We found agreement within experimental uncertainty for 2/3 of the cases (28 out of 42 shocks), but in the other 1/3 of the cases, to obtain an acceptable final solution, a more involved coordination of results of the two methods was required. We found that in approximately half of these (1/3) cases an acceptable normal was found using the more traditional averaging methods in the way described above. In the other cases the R-H method was the one that apparently provided the best results. Difficult to analyze IP shocks were listed and briefly discussed (Section 4); these were usually the result of non-steady input quantities.

There was a reduced number of fast IP shocks for many months centered around April 1996, which was near the minimum in ultraviolet radiance from the Sun. Also the shocks observed at solar minimum appeared weaker when measured by magnetosonic Mach number. A higher frequency of occurrence and a larger variety in shock strengths were observed before and after 1996. Most reverse shocks, associated with CIRs, were strong. The strongest shock observed of all those studied was a fast forward IP type just upstream of the magnetic cloud of October 18 - 19, 1995, and apparently was driven by the cloud.

We note that the shocks analyzed here cover more than two years near solar minimum. With a relatively quiet Sun it was possible to identify fast F and R IP shocks associated with CIRs and ICME (ejecta) separately; there was only one case of a F and R shock pair. Separations of types of the shock normals indicated that F(R) IP shocks during the solar minimum concentrated in a region in azimuth between approximately 170° and 210° (0° and 30°) but also extended further eastward (westward) covering the following azimuthal regions: $115° < \varphi_{GSE} < 225°$ for the F

cases and $-53° < \theta_{GSE} < 45°$ for the R cases. (Figure 7).

A Poisson distribution $F(r(\Phi_{GSE}),\lambda)$ of the distribution of the azimuthal directions for the F shocks, with a characteristic parameter $\lambda = 1.55$ and $\Phi_{GSE} = 220\pm10°$ (Equation 13), was shown to fit the azimuthal directions very well. The Poisson fit (Figure 8) to the orientations of the shocks with this value of Φ_{GSE} would suggest strong hindrance to shocks propagating upstream of a rather tightly winding Parker spiral. For CIRs the distribution of F shocks peaks at $<\varphi_{GSE}>$ ~ 194°. If this value of $<\varphi_{GSE}>$ for CIRs holds for a larger statistical set, it may indicate that CIRs that develop shocks at 1 AU are more tightly wound up than the average IMF at 1 AU having an azimuth of 45° from Parker theory (see e.g., Cravens [1997]). This value of $<\varphi_{GSE}>$ ~ 194° is closer to the azimuthal value of φ_{GSE} ~ 216°, corresponding to a winding field azimuthal angle of ~36°, given by the Acuña and Whang [1976] solar wind model, instead of the 45° winding angle of Parker.

The direction of the shock normals also peaked in, or near, the ecliptic plane, but some normals were observed to be broadly dispersed in latitude ($-75° < \theta_{GSE} < 70°$). All 8 shocks of unknown origin (i.e., not clearly driven by either CIR's or transients) had large inclinations with respect to the ecliptic plane ($<|\theta_{GSE}|> = 40°$), with only two cases occurring at lower and more moderate inclinations of approximately ± 20°.

The accurate determination of the θ_{Bn} angle is important for many studies. The characterization of the type of shock based in its obliquity angle θ_{Bn} depends on the accuracy of its determination, which obviously depends on the accuracies of both the estimated shock normal and the relevant upstream IMF. Often a non-steady state upstream IMF occurs making a good <IMF>-estimate unlikely or difficult, as emphasized in section 4. In our overall set of shocks as many as 10 cases (23%) had excellent estimates of θ_{Bn}; others range from poor to good (31% for each). [It is important to point out that the uncertainty on the estimate of θ_{Bn} is often more strongly dependent on the uncertainty of the estimate of the upstream IMF to use (which depends on the fluctuation/discontinuity content of the IMF) than on the uncertainty of the normal.] By obtaining these 10 excellent estimates of θ_{Bn} we hope, for example, to enable studies toward a more complete understanding of particle acceleration mechanisms at IP shocks, where accurate values of θ_{Bn} are crucial. Future studies using multiple spacecraft observations of IP shocks should help to increase the number of such excellent estimates of this important quantity, as well as many other improved shock parameter estimates.

The determination of the basic magnetohydrodynamic shocks parameters presented here may

facilitate the use of these shocks to further current efforts to better understand processes like the differentiated heating of minor ions; wave activity at quasi-parallel shocks; origin of the type-2 radio emissions; particle-energization; and other current topics of interest [see e.g. Berdichevsky et al., 1997; Gonzalez-Esparza et al., 1996; Thejappa et al. 1996, 1998; Lengyel-Fey et al., 1997; Giacalone et al., 1997; Baring et al., 1997; and references therein].

Acknowledgements

The compilation of the list of IP shocks greatly benefited from the available resources for plots of solar wind key parameters and plots of the orbit of WIND provided in the public domain Web pages, with URL: http://spof-www.gsfc.nasa.gov, by the ISTP/Science Planning and Operation Facility at Goddard Space Flight Center/NASA. We are indebted to Drs. P. Kellog, Z. Smith, D. Reames, N. Gopalswamy, and D. Larson who kindly helped us to complete the list of IP shocks observed with WIND. Finally, we acknowledge the support of the SWE and MFI instrument and data processing teams in this effort.

Appendix A

A description is presented of the shock normal recipes used with the pre-averaged methods.

In the determination of the magnetic coplanarity normal

$$\mathbf{n}_{MC} = \frac{(\mathbf{B}u - \mathbf{B}d)\times(\mathbf{B}u\times\mathbf{B}d)}{|(\mathbf{B}u - \mathbf{B}d)\times(\mathbf{B}u\times\mathbf{B}d)|} \tag{A1}$$

we avoid divide by zero, a common problem for perpendicular and parallel shocks, using the auxiliary vectors

$$\mathbf{t}_n = \frac{\mathbf{B}u\times\mathbf{B}d}{|\mathbf{B}u||\mathbf{B}d|} \tag{A2}$$

which is perpendicular to the coplanarity plane and

$$\mathbf{t}_t = \frac{(\mathbf{B}u - \mathbf{B}d)}{\sqrt{|\mathbf{B}u - \mathbf{B}d|^2}} \tag{A3}$$

defined along the direction tangent to the shock plane [Abraham-Schrauner and Yun, 1976]. This allows the determination of $\mathbf{n}_{MC}$ using the following unique set of two linear and one quadratic equations:

$$\mathbf{n}_{MC}\cdot\mathbf{t}_n = 0$$

$$\mathbf{n}_{MC}\cdot\mathbf{t}_t = 0 \tag{A4}$$

$$\mathbf{n}_{MC}^2 = 1$$

This system can be easily solved by expanding (A4) in any orthogonal system of coordinates.

The velocity coplanarity normal is evaluated using directly

$$\mathbf{n}_{VC} = \frac{\mathbf{V}d - \mathbf{V}u}{|\mathbf{V}d - \mathbf{V}u|} \tag{A5}$$

(**Vd-Vu**) is defined in the coplanarity plane [Abraham-Schrauner, 1972].

For the Abraham-Schrauner method there are several expressions to choose from [Abraham-Schrauner and Yun, 1976]. Our choice is

$$\mathbf{n}_{AS} = \mathbf{w}/|\mathbf{w}| \tag{A6}$$

with

$$\mathbf{w} = \left(\frac{(\mathbf{B}u - \mathbf{B}d)\times(\mathbf{B}u\times\mathbf{n}_{VC})}{|(\mathbf{B}u - \mathbf{B}d)\times(\mathbf{B}u\times\mathbf{n}_{VC})|} + \frac{(\mathbf{B}u - \mathbf{B}d)\times(\mathbf{B}d\times\mathbf{n}_{VC})}{|(\mathbf{B}u - \mathbf{B}d)\times(\mathbf{B}d\times\mathbf{n}_{VC})|}\right) \tag{A7}$$

This expression for $\mathbf{n}_{AS}$ is symmetric in the IMF upstream and downstream vectors. It also takes into account via (A5) the change in the direction of the plasma flow caused by the shock. This is evaluated using the same technique presented above for $\mathbf{n}_{MC}$.

Appendix B

For those cases where $\theta_{Bn} \neq 0$ the error in θ_{Bn} [$= \cos^{-1}(\mathbf{n} \bullet \mathbf{B}_{up}/B_{up})$] is evaluated via a Taylor expansion which assumes that the uncertainty $\Delta(\mathbf{n} \bullet \mathbf{B}_{up}/B_{up})$ is small. In this way we obtain the relationship

$$\Delta\theta_{Bn} = \Delta(\mathbf{n} \bullet \mathbf{B}_{up}/B_{up}) / \sqrt{(1 - [\mathbf{n} \bullet \mathbf{B}_{up}/B_{up}]^2)}$$

with

$$\Delta (\mathbf{n} \bullet \mathbf{B}_{up}/B_{up}) = (\Delta\mathbf{n}) \bullet \mathbf{B}_{up}/B_{up} + \mathbf{n} \bullet \Delta(\mathbf{B}_{up}/B_{up}),$$

where $\Delta\mathbf{n}$ includes the uncertainties associated with the Rankine-Hugoniot conditions (Equations 1 to 5) and its dependence on the selection of the upstream and downstream time intervals. $\Delta\mathbf{B}$ is given by the fluctuations $\delta\mathbf{B}$ around its mean value for the upstream region used for the derivation of $\mathbf{n}$, as indicated in Table 1 plus the experimental uncertainty $\varepsilon\mathbf{B}$, which in most cases is much smaller than $\delta\mathbf{B}$. For the special cases when $\theta_{Bn} \approx 0$, an ensemble of solutions θ_{Bn} is used, and the value of θ_{Bn} is the standard deviation from the mean value, evaluated for the ensemble of solutions used in the determination of $\Delta\mathbf{n}$.

References

Abraham-Shrauner, B., Determination of magnetohydrodynamic shock normals, *J. Geophys. Res.*, **77**, 736-739, 1972.

Abraham-Shrauner, B., and S. H. Yun, Interplanetary shocks seen by AMES plasma probe on Pioneer 6 and 7, *J. Geophys. Res.*, **81**, 2097-2102, 1976.

Acuña, M. H., L. F. Burlaga, R. P. Lepping, and N. F. Ness, Initial results from Voyagers 1, 2 magnetic field experiment, in *Solar Wind Four*, Ed. H. Rosenberger, p., 143, Rep. MPAE-100-81-31, Max-Plank Institute, Lindau, Germany, 1981.

Acuña, M. H. and Y. C. Whang, A two-region model of the solar wind including azimuthal velocity, *Astrophys. J.*, **203**, 720-738, 1976.

Balogh, A., J. Gonzalez-Esparza, R. Forsyth, M. Burton, B. Goldstein, E. J. Smith, and S. Bame,

Interplanetary shock waves: Ulysses observations in and out of the ecliptic plane, *Space Sci. Rev.*, **72**, 171-180, 1995.

Balogh, A., P. Riley, Overview of heliospheric shocks, in *Cosmic Winds and the Helioshere*, (eds.) J. R. Jokipii, C. P. Sonnett, and M. S. Gianpapa, The University of Arizona Press, Tucson Arizona, p. 359, 1997.

Baring, M.G, K.W. Ogilvie, D.C. Ellison, and R.J. Forsyth, Acceleration of solar wind ions by nearby interplanetary shocks: comparison of Monte Carlo simulations with Ulysses observations, Astrophys. J., **476**, 889-902, 1997

Bavassano-Cattaneo, M. B., B. T. Tsurutani, E. J., Smith, and R. P. Lin, Subcritical and super-critical shocks: Magnetic field and energetic particle observations, *J. Geophys. Res.*, 91, 11929-11935, 1986.

Berdichevsky, D., J. Geiss, G. Gloeckler, and U. Malls, Excess heating of $4He^{++}$ and $O6^{+}$ relative to H+ downstream of interplanetary shocks, *J. Geophys. Res.*, **102**, 2623-2635, 1997.

Berdichevsky, D., J.-L. Bougeret, J.-P. Delaboudinie, N. Fox, M. Kaiser, R. P. Lepping, D. Michels, S. Plunkett, D. Reames, M. Reiner, I. Richardson, G. Rostoker, J. Steinberg, B. Thompson, and T. von Rosenvinge, Evidence for multiple ejecta; April 7-11, 1997 ISTP Sun-Earth Connection Event, *Geophys. Res. Lett*, **25**, 2473 - 2476, 1998.

Borrini, G., J. T. Gosling, S. J. Bame, An analysis of shock wave disturbances observed at 1 AU from 1971 through 1978, *J. Geophys. Res.*, **89**, 5381, 1982.

Bougeret, J.-L., Observations of shock formation and evolution in the solar atmosphere, eds., B. T. Tsurutani and R. G. Stone, *Collisionless Shocks in the Heliosphere: Reviews of Current Research*, AGU Monograph no. **35**, Washingtion DC, 13 - 32, 1985.

Burgess, D., Collisionsess Shocks, *Introduction to Space Physics*, eds., M. G. Kivelson and C. T. Russell, Cambridge Univ. Press, pp 129 - 163, 1995.

Burlaga, L. F., Interplanetary stream interfaces, *J. Geophys. Res.*, **79**, 3717-3725, 1974.

Burlaga, L., E. Sittler, F. Mariani, and R. Schwenn, Magnetic loop behind an interplanetary shock: Voyager, Helios, and IMP-8 observations, *J. Geophys. Res.*, **86**, 6673, 1981.

Burlaga, L, K. Behannon, and L. W. Klein, Compound streams, magnetic clouds and major magnetic storms, *J. Geophys. Res.*, **92**, 5725, 1987.

Burlaga, L., *Interplanetary Magnetohydrodynamics*, Ed. Oxford University Press, N. Y., 1995.

Burlaga, L., R. Fitzenreiter, R. Lepping, K. Ogilvie, A. Szabo, A. Lazarus, J. Steinberg, G. Gloecker, R. Howard, D. Michels, C. Farrugia, R. P. Lin, and D. E. Larson, A magnetic claud containing prominence material: January 1997, *J. Geophys. Res.*, **103**, 277-286, 1998.

Cane H. V., N. R. Sheeley, and Jr., and R. A. Howard, Energetic interplanetary shocks, radio emissions, and coronal mass ejections, *J. Geophys. Res.*, **92**, 9869-9874, 1987.

Cane H. V., I. G. Richardson, and O. C. St. Cyr, The interplanetary events of January-May 1997, as inferred from energetic particle data, and their relationship with solar events, *Geophys. Res. Lett.*, *25*, 2517-2520, 1998.

Cane H. V., D. V. Reames, and T. T. von Rosenvinge, The role of interplanetary shocks in the longitude distribution of solar energetic particles, *J. Geophys. Res., 93*, 9555-9567, 1988.

Dryer, M., Interplanetary studies: Propagation of disturbances between the Sun and the magnetosphere, *Space Sci. Rev.*, *67*, 363-419, 1994.

Ellison, D. C., M. G. Baring, and F. C. Jones, Acceleration rates and injection efficiencies in oblique shocks, Astrophys. J., ***453***, 873-882, 1995.

Giacalone J., D. Burgess, S.J. Schwartz, D.C. Ellison, and L. Bennett, Injection and acceleration of thermal protons at quasi-parallel shocks: A hybrid simulation parameter survey, J. Geophys. Res., 19789-19804, 1997

Gold, T., Contribution to discussion, in *Gas Dynamics of Cosmic Clouds*, Eds. H.C. van de Hulst and J.M. Burgers, p. 103, North-Holland, Amsterdam, 1955.

Gonzalez, W. D., B. T. Tsurutani, A. L. C. Gonzalez, E. J. Smith, F. Tang, and S.-I. Solar wind magnetosphere coupling during intense magnetic storms (1978-1979), *J. Geophys. Res.*, ***94***, 8835, 1989.

Gonzalez-Esparza, J.A., E.J. Smith, A. Balogh, and J.L. Phillips, The quasi-parallel shock wave detected by Ulysses on day 92:109, Astron. Astrophys., **316**, 323-332, 1996

Gopalswamy, N, M. L. Kaiser, R. P. Lepping, S. W. Kahler, K. Ogilvie, D. Berdichevsky, T. Kondo, T. Isobe, and M. Akioka, Origin of coronal and interplanetary shocks: A new look with WIND spacecraft data, *J. Geophys. Res.*, ***103***, 307-316, 1998.

Gopalswamy, N., Y. Hanoaka, T. Kosugi, R. P. Lepping, J. T. Steinberg, S. Plunkett, R. A. Howard, B. J. Thompson, J. Gurman, G. Ho, N. Nitta, and H. S. Hudson, *Geophys. Res. Lett.*, ***25***, 2485-2488, 1998.

Gosling, J. T., A. J. Hundhausen, V. Pizzo, and J. R. Asbridge, Compression and rarefactions in the solar wind: Vela 3, *J. Geophys. Res., 77*, 5442-5454, 1972.

Gosling, J. T., E. Hildner, R. M., MacQueen, R. H. Munro, A. I. Poland, and C. L. Ross, Mass Ejections from the Sun; A view from Skylab, *J. Geophys. Res., 79*, 4581-4586, 1974.

Gosling, J. T., Solar wind stream evolution, Solar wind four, Ed. H. Rosenbauer, *Report no. MPAE-W-100-81-31*, 107-117, 1981.

Gosling, J. T., and A. E. Robson, Ion reflection, gyration, and dissipation at supercritical shocks, eds. B. T. Tsurutani and R. G. Stone, *Collisionless Shocks in the Heliosphere: Reviews of Current Research*, AGU Monograph no. **35**, Washingtion DC, 141 - 152, 1985.

Hundhausen, A. J., The solar wind, in *Introduction to Space Physics*, edited by M. G. Kivelson and C. T. Russell, Cambridge Univ. Press, New York, **91**, 1995.

Jordanova V., C. Farrugia, L. Janoo, J. Quinn, R. Torbet, K. Ogilvie, R. P. Lepping, J. Steinberg, D. McComas, and R. Belian, October 1995 magnetic cloud and accompanying storm activity: Ring current evolution, *J. Geophys. Res.*, ***103***, 79-92, 1998

Lario, D., Propagation of low-energy particles through the interplanetary medium: modeling their injection from interplanetary shocks, Dissertation: Doctor en Cices F siques, Depart-ament d'Astronomia i Meteorologia, Universitat de Barcelona, Spain, 1997.

Lepping, R. P., and P. D. Argentiero, Single spacecraft method of estimating shock normals, *J. Geophys. Res.*, ***76***, 4349-4359, 1971.

Lepping, R. P., M. H. Acuña, L. F. Burlaga, W. M. Farrell, J. A. Slavin, K. H. Schatten, F. Mariani, N. F. Ness, F. M. Neubauer, Y. C. Whang, J. B. Byrnes, R. S. Kennon, P. V. Panetta, J.

Scheifele, and E. M. Worley, The WIND Magnetic Field Investigation, *Space Science Rev.*, ***71***, 207-229, 1995.

Lepping, R. P., L. F. Burlaga, A. Szabo, K. W. Ogilvie, W. H. Mish, D. Vassiliadis, A. J. Lazarus, J. T. Steinberg, C. J. Farrugia, L. Janoo, and F. Mariani, The WIND magnetic cloud and events of October 18-20, 1995: Interplanetary properties and as triggers for geomagnetic activity, *J. Geophys. Res.*, ***102***, 14049-14063, 1997.

Lepping, R. P., D. Berdichevsky, A. Szabo, L. F. Burlaga, B. J. Thompson, F. Mariani, A. J. Lazarus, J. T. Steinberg, Typical and Unusual properties of magnetic clouds during the WIND era, SH51A-08 abstract, *EOS Transactions*, AGU Spring Meeting, p. S267, 1999.

Lengyel-Frey, D., G. Thejappa, R. J. MacDowall, R. G. Stone, and J. L. Phillips, Ulysses observations of wave activity at interplanetary shocks and implications for type II radio bursts, *J. Geophys. Res.*, ***102***, 2611-2622, 1997.

Mish, W., J. Green, M. Reph, and M. Peredo, ISTP science data systems and products, *Space Sci. Rev.*, ***71***, 815-878, 1995.

Ogawa, H. S., D. L. Judge, D. R. McMullin, D. Gangopadhyay, A. B. Galvin, *J. Geophys. Res.*, ***103***, 1 - 6, 1998.

Ogilvie, K. W., D. J. Chornay, R. J. Fitzenreiter, F. Hunsaker, J. Keller, J. Lobell, G. Miller, J. D. Scudder, E. C. Sittler, R. B. Torbert, D. Bodet, G. Needell, A. J. Lazarus, J. T. Steinberg, J. H. Tappan, A. Mavretic, and E. Gergin, SWE, A Comprehensive Plasma Instrument for the Wind Spacecraft, *Space Science Rev.*, ***71***, 55-77, 1995.

Peredo, M., S. Boardsen, D. Berdichevsky, and G. Galiardi, New ISTP products on the Wide Web Server, ISTP Newsletter, **6**, (2)33-(2)34, 1996; electronically at http://www-istp.gsfc.nasa.gov/istp/newsletter.html

Pizzo, V. J., An evaluation of corotating stream models, in *Solar Wind Four,* Ed. H. Rosenbauer, p. 153, MPAE-100-81-31, 1981.

Reames, D. V., L. M. Barbier, and C. K. Ng, The spatial distribution of particles accelerated by coronal mass ejection-driven shocks, *Astrophys. J.*, ***466***, 473-386, 1996.

Reames, D. V., L. M. Barbier, T. T. von Rosenvinge, G. M. Mason, J. E. Mazur, and J. R.

Dwyer, Energy spectra of ions accelerated in impulsive and gradual solar events, *Astrophys. J.*, ***483***, 515-522, 1997.

Reiner, M. J., M. L. Kaiser, J. Fainberg, J.-L. Bougeret, and R. G. Stone, On the origin of radio emissions associated with the January 6-11, 1997 CME, *Geophys. Res. Letts.*, in press, 1998.

Richardson, I. G., and H. V. Cane, Signatures of shock drivers in the solar wind and their dependence on the solar source location, *J. Geophys. Res.*, ***98***, 15295, 1993.

Richter, A. K., K. C. Hsieh, H. Rosenbauer, and F. M. Neubauer, Parallel fast-forward shock waves within 1 AU: Helios-1 and -2 observations, *Ann. Geophys.*, ***4***, 1, 1986.

Sanderson, T. R., R. P. Lin, D. Larson, M. P. McCarthy, G. K. Parks, J. Bosqued, N. Lormant, K. Ogilvie, R. Lepping, A. Szabo, A. Lazarus, J. Steinberg, J. Hoeksema, Wind observations of the influence of the Sun's magnetic field on the interplanetary medium at 1 AU, *J. Geophys. Res.*, ***103***, 17, 235, 1998.

Scudder, J. D., L. F. Burlaga, and E. W. Greenstadt, Scale lengths in quasi-parallel shocks, *J. Geophys. Res.*, ***89***, 7545, 1984.

Silverman, S. M., Low latitude auroras: the storm of September 25, 1909, *J. Atmos. Terr. Phys.*, ***57***, 673, 1995.

Steinolfson, R. S., M. Dryer, and Y. Nakagawa, Interplanetary shock pair disturbances: Comparison of theory with space probe data, *J. Geophys. Res.*, ***80***, 1989-2000, 1975.

Smith, Z, and M. Dryer, Numerical simulations of high-speed solar wind streams within 1 AU and their signatures at 1 AU, *Solar Phys.*, ***131***, 363-383, 1991.

Szabo, A., An improved solution to the "Rankine-Hugoniot" problem, *J. Geophys. Res.*, ***99***, 14737-14746, 1994.

Thejappa, G., R. J. MacDowall and R. G. Stone, Unusual Wave Activity near Interplanetary Shocks, SOLAR WIND EIGHT, AIP Conference Proceedings, 382, (ed.) Daniel Winterhalter et al., p. 393, 1996.

Thejappa, G., R. J. MacDowall, and A.F. Viñas, In situ Wave Phenomena in the Upstream and Downstream regions of Interplanetary Shocks: Implications for Type II Burst Theories, In the Proceedings of ESLAB Symposium no. 13, in press, 1998.

Tidman, D. A., and N. A. Krall, *Shock Waves in Collisionless Plasmas*, in Wiley Series in Plasma Physics, Ed. Wiley-Interscience, New York, 1971.

Viñas, A. F., J. Scudder, Fast and optimal solution to the "Rankine-Hugoniot Problem, *J. Geophys. Res.*, ***91***, 39-58, 1986.

Watari, S., and T. Watanabe, The solar drivers of geomagnetic disturbances during solar minimum, *Geophys. Res. Lett.*, ***25***, 2489-2492, 1998.

Whang, Y. C., J. Zhou, R. P. Lepping, and K. W. Ogilvie, Interplanetary slow shock observed from WIND, *Geophys. Res. Lett.*, ***23***, 1239-1242, 1996.

Zwickl, R. D., Asbridge, S. J., Bame, W. C. Feldman, J. T. Gosling, and E. J. Smith, Plasma properties of driver gas following interplanetary shocks observed by ISEE-3, SOLAR WIND FIVE, NASA Conf. Publ., CP-2280, 711, 1983.

Table 1: List of shocks, average-method technique

Sh. No.	Year	Date/Time MMDD hhmm	intervals up(stream) hhmm-	dw(stream) hhmm-	shock normal ϕ_n in [°]	θ_n [GSE]	V_s relative to up SW [km/s] and shock type		IMF Bup ϕ_B in [°]	θ_B [GSE]	|Bup| in [nT]	θBn in [°]	Agreement within ≤15° bw. shock n
1	94	12/5 2101	2036-2054	2106-2124	213±1	19±2	122±10	F	103±5	15±11	10.0±1.5	76±5°	mc, vc, AS
2	95	1/1 1936	***-***	***-***	**	**	**	F	**	**	***	***	none
3	95	3/4 0037	0028-0031	0038-0041	202±1	46±1	94±8	F	270±1	17±0.5	4.1±0.2	88-90°	vc, AS
4	95	3/12 0220	0221-0226	0200-0220	307±14	54±2	194±20	R	288±13	-21±23	7.5±2.5	75±15°	mc, vc, AS
5	95	3/23 0937	0912-0921	0945-0952	157±3	-12±2	95±10	F	84±2	-41±4	3.9±0.2	69±6°	vc, AS
6	95	4/7 2020	2030-2036	2013-2018	18±1	5±1	166±17	R	345±13	17±16	4.6±1.2	34±20°	mc, vc, AS
7	95	5/2 2357	3 0006-0018	2 2351-2357	26±1	-6.5±1	178±20	R	37±13	-8±19	6.8±1.7	11±10°	mc, vc, AS
8	95	5/24 0439	0512-0530	0430-0439	16±3	0±1	106±15	R	142±11	25±19	7.4±2.0	57±14°	vc, AS
9	95	6/26 0340	0354-0406	0336-0342	31±2	-29±1	171±20	R	299±6	-23±14	6.3±2.0	81±15°	vc, AS
10	95	7/24 0223	0206-0221	0224-0233	205±11	3±1	78±10	F	176±19	19±14	2.0±0.4	33±17°	mc, vc, AS
11	95	8/22 1256	1245-1254	1258-1304	151±4	28±1	77±10	F	290±12	20±14	2.1±0.5	62±8°	mc, vc, AS
12	95	8/24 2211	2203-2209	2212-2221	189±3	-26±2	70±7	F	250±4	20±13	6.6±1.0	75±10°	mc, vc, AS
13	95	10/18 1041	1034-1040	1042-1045	205±3	-12±6	96±30	F	85±68	0-90	**$0.7\pm1.2_s$**	**0-85°**	poor, vc/IMC V
14	95	10/19 1751	***	***	**	**	**	F	**	**	***	88-90°	use mple. S/C†
15	95	10/22 2120	2114-2117	2124-2127	117±1	48±1	110±7	F	104±3	0±6	4.4±0.1	53±2°	mc, AS
16	95	11/27 0822	0754-0806	0823-0828	173±1	-35±0.5	50±3	F	87±3	-10±3	3.6±0.2	81±8°	vc, AS
17	95	12/15 0437	0424-0432	0439-0448	157±1	12.5±1	40±2	F	316±4	13±8	3.4±0.4	33±2°	mc, AS
18	95	12/24 0558	0536-0549	0600-0609	209±2	-13±1	95±7	F	141±16	-9±14	6.5±1.6	71±15°	mc, vc, AS
19	95	12/25 2304	2304-2310	2255-2301	323±3	-7±5	56±12	R	150±7	32±19	6.0±1.8	25±13°	mc, AS
			2304-2310	2255-2301	336±2	19±5	60±14		150±7	32±19	6.0±1.8	51±10°	vc, AS
20	96	2/6 1912	1848-1900	1915-1925	194±1	9.7±1	50±2	F	17±0.6	23±2	4.1±0.2	33±5°	mc, AS
21	96	2/21 2210	2148-2200	2215-2218	180±4	62±3	52±5	F	352±6	11±3	3.0±0.2	73±4°	mc, AS
22	96	4/2 1007	0954-1006	1009-1013	132±1	48±1	56±2	F	4.7±0.1	10±3	2.7±0.3	74±3°	mc, vc, AS
23	96	4/3 0947	0941-0946	0949-0952	204±2	32±3	54±4	F	112±2	25±2	4.4±0.2	79±1°	mc, vc, AS
24	96	4/8 0241	0230-0240	0242-0249	210±3	52±2	67±6	F	138±5	15±2	5.7±0.4	67±2°	mc, AS
25	96	6/18 2236	2228-2234	2236-2242	163±1	8±0.5	73±3	F	253±3	-15±7	7.6±0.8	85-90°	vc, AS
26	96	7/28 1215	1210-1213	1215-1218	196±1	-28±1	52±2	F	143±10	9±5	$2.0\pm0.2_s$	63±6°	vc, AS
27	96	9/26 2136	2137-2140	2134-2136	356±1	-18±1	140±7	R	75±0.5	14±17	4.0±0.6	80-90°	vc, AS

Notice that the shock normal points upstream of the shock; **mc** = magnetic coplanarity, **vc** = velocity coplanarity, **AS**=Abrahm-Schrauner
† see Lepping et al., [1997]

Table 1: (continuation)

Sh. No.	Year	Date/Time MMDD hhmm	intervals upstream	dwstream	shock normal ϕn in [°]	θn [GSE]	V_s relative to up SW [km/s] and shock type		IMF **B** ϕ_B in [°]	θ_B [GSE]	|Bup| [nT]	θBn	Agreement within ≤15° bw. shock n
28	96	12/2 1000	0952-0958	1000-1006	169±3	21±2	60±7	F	149±3	36±10	4.7_5±0.6	24±5°	vc, AS
29	96	12/9 1850	1814-1843	1910-1941	188±2	-4±5	40±20	F	164±19	26±27	2.2_5±0.8	**34±17°?**	mc, AS
30	97	1/10 0052	0030-0042	0055-0104	196±6	-32±5	75±8	F	161±4	8±7	2.2±0.3	53±9°	mc, vc, AS
31	97	1/28 0854	0855-0901	0847-0853	25±20	-60±10	171±20	R	3.3±12	44±9	**5.8±0.7**	**70±20°**	poor, vc≈mc
			0855-0901	0847-0853	14±15	-80±10	165±20		3.3±12	44±9	**5.8±0.7**	**56±20°**	poor w. AS
32	97	2/9 1250	1242-1246	1300-1304	172±2	5±2	114±12	F	204±9	30±11	3.6±0.6	39±8°	mc, vc, AS
33	97	3/5 1255	1233-1239	1258-1304	184±1	-10±1	77±5	F	348±6	29±8	4.5±0.5	24±9°	mc, AS
34	97	3/20 1910	1927-1939	1948-2000	194±1	52±0.5	53±4	F	72±2	29±8	3.1±0.4	84±2°	vc, AS
35	97	3/23 0821	0800-0818	0824-0836	205±20	65±8	72±12	F	291±17	-20±24	2.0±0.6	73±12°	mc, vc, AS
36	97	4/10 1255	1240-1245	1259-1302	160±5	51±3	91±10	F	330±20	45±12	7.0±1.5	85±4	vc, AS.
37	97	4/11 2052	2100-2115	2047-2055	34±1	27±1	55±6	R	91±2	-38±9	4.9±0.6	75-90°	vc, AS
38	97	5/1 1205	1148-1200	1206-1212	215±10	45±6	64±7	F	14±0.5	-11±32	2.0±0.8	43±20°	mc, vc, AS
39	97	5/15 0115	0048-0112	0115-0121	208±0.5	-19±1	121±10	F	113±2	-17±5	7.2±0.5	84-90°	vc, AS
40	97	5/20 0512	0448-0500	0512-0524	166±5	-26±3	59±5	F	142±9	-28±11	3.4±0.8	13±4°†	mc, AS
41	97	5/25 1345	1336-1348	1354-1406	185±10	-20±3	66±8	F	103±18	37±16	4.8±1.3	70-90°	vc, AS
42	97	5/26 0916	0900-0915	0918-0921	180±7	-27±6	61±9	F	158±1	-8±21	2.5±0.5	38±22°	2pts dw, mc,AS

Notice that the shock normal points upstream of the shock; **mc** = magnetic coplanarity, **vc** = velocity coplanarity, **AS**=Abrahm-Schrauner

† $\Delta\theta_{Bn}$ evaluated using the root mean square standard deviation for a distribution of solutions, $\{\theta_{Bn}\}$, see Appendix B.

Table 2: Final solution to the shock problem
(pre-averaged methods and non-linear solution to the R-H shock problem)

Sh. No.	Year	Date MMDD	Shock Type	shock normal ϕn in [°] GSE	θn	Vs (up) km/s	θBn (up)
1	94	12/5	F Q⊥	214±3	17±3	120±20	76±5°
2	95	1/1	F	190±12	10±8	61±10	43±7°
3	95	3/4	F Q⊥	202±2	44±2	94±7	85-90°
4	95	3/12	R Q⊥	4±15	54±4	200±20	75±15°
5	95	3/23	F Q⊥	170±6	-15±4	90±5	69±6°
6	95	4/7	R	4±18	6±8	160±20	34±20°
7	95	5/2	R Q//	13±10	-7±2	150±40	24°±13°
8	95	5/24	R Q//	6±10	-1±2	160±20?	57±14°
9	95	6/26	R Q⊥	15±16	-25±4	140±35	70-90°
10	95	7/24	F Q//	206±14	2±2	80±8	33±17°
11	95	8/22	F	147±7	30±2	75±10	62±8°
12	95	8/24	F Q⊥	185±5	-21±5	73±8	75±10°
13	95	10/18	F Q//?	202±9	-9±7	110±20	**0-85°**
14	95	10/19	F Q⊥	128	21	137±5	88-90°
15	95	10/22	F Q⊥	120±7	48±3	110±25	53±6°
16	95	11/27	F Q⊥	182±10	-48±12	60±10	81±8°
17	95	12/15	F	**162±5**	**13±3**	39±7	33±2°
18	95	12/24	F	205±4	-15±2	100±10	71±15°
19	95	12/25	R Q⊥	353±17	27±8	125±15	51±10°
20	96	2/6	F Q//	188±6	16±12	52±8	33±5°
21	96	2/21	F Q⊥	185±7	45±15	45±12	73±4°

Table 2: (continuation)

Sh. No.	Year	Date MMDD	Shock Type	shock normal ϕ_n	θ_n	Vs (up)	θ_{Bn} (up)
				in [°] GSE		km/s	
22	96	4/2	F Q⊥	156±24	55±7	50±15	74±3°
23	96	4/3	F Q⊥	202±2	25±8	52±10	79±1°
24	96	4/8	F Q⊥	213±3	50±3	70±7	67±2°
25	96	6/18	F Q⊥	168±5	4±4	75±15	85-90°
26	96	7/28	F	187±10	-24±5	60±20	63±12°
27	96	9/26	R Q⊥	18±22	-25±7	140±15	80-90°
28	96	12/2	F Q//	169±3	21±2	55±16	24±5°
29	96	12/9	F Q//	194±10	-6±7	40±10	**0-65°**
30	97	1/10	F	200±3	-30±3	75±8	51±9°
31	97	1/28	R Q⊥	-20±40	70±15	150±60	70±15°
32	97	2/9	F Q//	196±26	5±5	115±13	59±28°
33	97	3/5	F Q//	184±1	-10±1	77±6	24±2°
34	97	3/20	F Q⊥	194±1	52±0.5	54±3	84°±13°
35	97	3/23	F Q⊥	199±8	58±3	72±10	73±12°
36	97	4/10	F Q⊥	160±7	51±5	91±10	85±5°
37	97	4/11	R Q⊥	18±20	27±1	56±10	75-90°
38	97	5/1	F	217±2	49±2	64±6	43±20°
39	97	5/15	F Q⊥	208±0.5	-19±1	121±10	84-90°
40	97	5/20	F Q//	190±20	-15±12	58±6	15±8°
41	97	5/25	F Q⊥	185±2	-20±1	73±7	70-90°
42	97	5/26	F Q//	176±14	-26±7	60±9	38±22°

Table 3. Statistical results R-H shock parameters

Mean IP shock properties	All IP shocks	F IP shocks	R IP shocks	CIR driven (F)	t. driven (F)	Unknown driver
|V| relat. up region	90 ± 40 km/s	78 ± 28 km/s	145 ± 42 km/s	72 ± 23 km/s	91 ± 26 km/s	57 ± 10 km/s
Vx GSE.	- 426 ± 81 km/s	- 397 ± 63 km/s	- 524 ± 56 km/s	- 382 ± 42 km/s	- 412 ± 84 km/s	- 380 ± 43 km/s
Vy GSE	- 2 ± 42 km/s	- 16 ± 30 km/s	35 ± 43 km/s	- 24 ± 27 km/s	- 6 ± 31 km/s	2 ± 30 km/s
Vz GSE	0 ± 48 km/s	5 ± 37 km/s	7 ± 71 km/s	13 ± 31 km/s	8 ± 71 km/s	14 ± 48 km/s
Ms (magnetosonic)	1.44±0.35	1.39±0.34	1.66±0.345	1.31±0.26	1.66±0.40	1.125±0.08
ϕ_{GSE_n} (azimuth)	———	185±23°	9±31°	193±23°	175±21°	180±30°
θ_{GSE_n} (latitude)	8±32°	13±30°	0±37°	22±30°	2±29°	(<|θ|>) 40±15°
θBn	59±24°	62±21°	60±22°	57±22°	54±28°	72±15°

The definition of the quantities (Q) are given in column 1, and for their respective distribution of values Columns 2 to 7 present the mean <Q> plus/minus the standard deviation σ(Q).

Table 4a: (strong shocks)

Sh. No.	Year	Date MMDD	Vs [Earth Sys.] km/s [GSE] Vx Vy Vz	V_s/V_A up	M_s up	Driver
1	94	12/5	-443. -76. 25.	2.4	1.8^{+}	CIR
3	95	3/4	-474, -8, 33	2.6	1.5_{s}	MC
4	95	3/12	-582, -17, 124	2.8	1.8	CIR
5	95	3/23	-375, 4., -30.	3.6	1.8	t?
6	95	4/7	-536 84 -15	3.4	2.0^{+}	CIR
7	95	5/2	-599 45 -77	2.1	1.6^{+}	CIR
8	95	5/24	-506 38 -30	2.3	1.6	CIR
9	95	6/26	-429 77 -47	3.0	2.0^{+}	CIR
10	95	7/24	-386 -50 15	6.5	1.9	t?
13	95	10/18	-408, -36, -18	24.	2.4	MC
15	95	10/22	-433, 30, 84	3.0	1.9^{+}	t
27	96	9/26	-542., 38, -123	2.4	1.5^{+}	CIR
30	97	1/10	-439, -31, -18,	4.2	1.5	MC
31	97	1/28	-546 71 -95	2.4	1.8	CIR
32	97	2/9	-632, 44, -26	3.4	1.7^{+}	t
33	97	3/5	-393, -17., -24.	3.7	1.6^{+}	CIR
36	97	4/10	- 359, 5.5, 77.	2.2_{s}	1.45	t
39	97	5/15	-422, -70, -58	3.8	2.1_{s}	MC

CIR = Corotating interactive region; MC = Magnetic Cloud; t = other transient

Table 4b: (weak shocks)

Sh. No.	Year	Date/Time MMDD hhmm	Vs [Earth Sys.] km/s [GSE] Vx	Vy	Vz	V_s/V_A up	M_s up	Driver
2	95	1/1	-376	-10	9	3.2	1.3	CIR
11	95	8/22	-381.,	12.,	44.,	3.1	1.4_5	MC
12	95	8/24	-385,	-6.,	-20.	2.4	1.4_5	CIR
14	95	10/19	-467.,	72.,	52.	1.45	1.3	?
16	95	11/27	-342	1	-84	2.5	1.0_5	?
17	95	12/15	-346	24	-1	2.2	0.9_5	MC
18	95	12/24	-416	-85	-54	2.6	1.4	CIR
19	95	12/25	-509	-28	71	5.3	1.4	CIR
20	96	2/6	391	-11	7	1.7	1.0_3	CIR
21	96	2/21	-422	-3	20	2.2_5	1.0_5	?
22	96	4/2	-359	9	45	3.3	1.1_2	?
23	96	4/3	-380	-20	22	2.4	1.1	?
24	96	4/8	-318	-49	49	2.3_5	1.2	CIR
25	96	6/18	-478	-5	-6	1.5	1.1	CIR
26	96	7/28	-355	-32	-22	5.0	1.2-1.4	CIR
28	96	12/2	-329	-11	15	2.4	1.2	t?
29	96	12/9	-370	-20	$-0._5$	3.5	~ 1	CIR
34	97	3/20	-337	-16	43	3.5	1.1	?
35	97	3/23	-378,	-14,	53	4.2	1.4	CIR
37	97	4/11	-510	46	27	1.5	1	t?
38	97	5/1	-372	-17	43	5.4	1.25	?
40	97	5/20	-344	16	-32	3.	1.2	t?
41	97	5/25	-363	-6	-32	2.3	1.2	?
42	97	5/26	-339	-10	-36	3.6	1.25	t

CIR = Corotating interactive region; MC = Magnetic Cloud; t = other transient

Figure Captions

Figure 1. (a,b,c for April 7, 1995 [Shock no. 6 in Table 1] and June 26, 1995 [Shock no. 9] and June 18, 1996 [Shock no. 25], respectively) Histograms of shock normal directions based on three different analysis methods in terms of longitude (or azimuth, φ_n) and latitude (θ_n) for many chosen analysis-intervals for each of the events. The methods used in analyzing the shocks are: magnetic-coplanarity (mc), velocity-coplanarity (vc), and the Abraham-Shrauner (AS) mixed method.

Figure 2. Examples of R-H fit results (solid lines are the asymptotic solutions with 1σ error estimates shown by dotted lines), superimposed on the data employed. For June 26, 1995, reverse (a) and June 18, 1996 forward (b), shocks. Shown are (in order from top to bottom) : (1) N_p, proton number density, (2,3,4) Vx,y,z(GSE) components of the solar wind bulk speed, (5) thermal speed, and (6,7,8) the Bx,y,z(GSE) components of the IMF. Note the close agreement between the measurements and fit results.

Figure 3. Confidence regions for R-H shock normal fittings. Panel a) shows 1,2,3, and 4 sigma regions around the best fit normal of the 1995 June 26 shock. Panel b) shows the same confidence regions for the 1996 June 18 shock illustrating that uncertainties might by distributed anisotropicaly. The unit sphere with the pole along the GSE x axis and the prime meridian in the GSE Y direction, represent the locus of possible shock normal directions. For stable solutions the confidence regions are small and show an approximately concentric area around the best fit solution, as in case (a).

Figure 4. The longitude (φ, top panel) and latitude (θ, bottom panel) of the estimated IP shock normals vs. time for the p-average technique (open triangles) and the R-H method (closed inverted triangle). In general the two techniques agree quite well.

Figure 5. (Open circles): A comparison of the resulting shock normals from the "averaging" (p-ave) method and Rankine-Hugoniot (R-H) fitting method in terms of the cosine of the angle between the normals (i.e., $\mathbf{n}_{p\text{-}ave} \cdot \mathbf{n}_{R\text{-}H}$). (Notice that on the right side is shown the corresponding angles.) (Closed circles): A similar comparison of the sum of the cosine of the angle between the normals and the (assumed positive) error in their estimates (i.e., $\Delta(\mathbf{n}_{p\text{-}ave} \cdot \mathbf{n}_{R\text{-}H})$); note that the closed circles are necessarily higher than the open circles.

Figure 6. (a) Distribution of shock speeds, i.e., magnitude of shock velocity with respect to the upstream solar wind bulk velocity. (b) Upstream magnetosonic Mach number (M_S) vs. time showing an unexplained dip for about 6 months centered at early April 1996; the intervals

between adjacent tick marks on the horizontal are about 2 months long.

Figure 7. Polar distribution of the shock surface normal (**n**) orientations projected into the ecliptic plane (GSE coordinates), for forward (F) and reverse (R) shocks separately. The arrows indicate the average direction of the F (pointing approximately left-ward) and R (right-ward) cases. Notice that only the x,y projections (i.e., into the Ecliptic plane) of the normals are shown, i.e., $\langle \mathbf{n}_{X,Y}(F) \rangle = \langle \mathbf{n}(F) \rangle - \langle \mathbf{n}_Z(F) \rangle$, and likewise for the reverse (R) shock normals. Notice also the paucity of cases in the extreme dawn and dusk directions.

Figure 8. Histograms of GSE longitude (φ) for Forward (F - panel a) and Reverse (R - panel b) shock normals. Similarly (in panel c) a histogram of latitude (θ) of all of the interplanetary shock normals. The striped area represents the shocks associated with CIR's and the dark areas are those shocks driven by transients. The inverted triangles are the result of a least-squares fitted Poisson distribution (see text).

Figure 9. Histogram of longitudes (φ) and latitude (θ) for forward (F) IP shock surface normals (**n**) for the cases of: (Top) those driven by CIR's: (Middle) those driven by transients such as magnetic clouds; and (Bottom) those for whom the driver or origin is unknown.

Figure 10. (Top panel): Histogram of the angle between the shock normal and the upstream magnetic field direction, θ_{Bn}. (Bottom panel): θ_{Bn} vs. magnetosonic Mach number (M_s).

Figure 11. An example (December 9, 1996) of a pulsation shock in terms of (in the top three panels): 3 s averages of the magnetic field, where $|\mathbf{B}|$is field magnitude, and φ_B and θ_B are the longitude and latitude angles of the field, respectively, in a GSE Cartesian system, and (in the bottom three panels) 92 s spaced ~15 s plasma quantity averages: N_p is the proton number density, $|\mathbf{V}|$is the solar wind speed, and V_{Th} is the proton thermal speed. The vertical dashed line indicates the estimated position of the shock ramp.

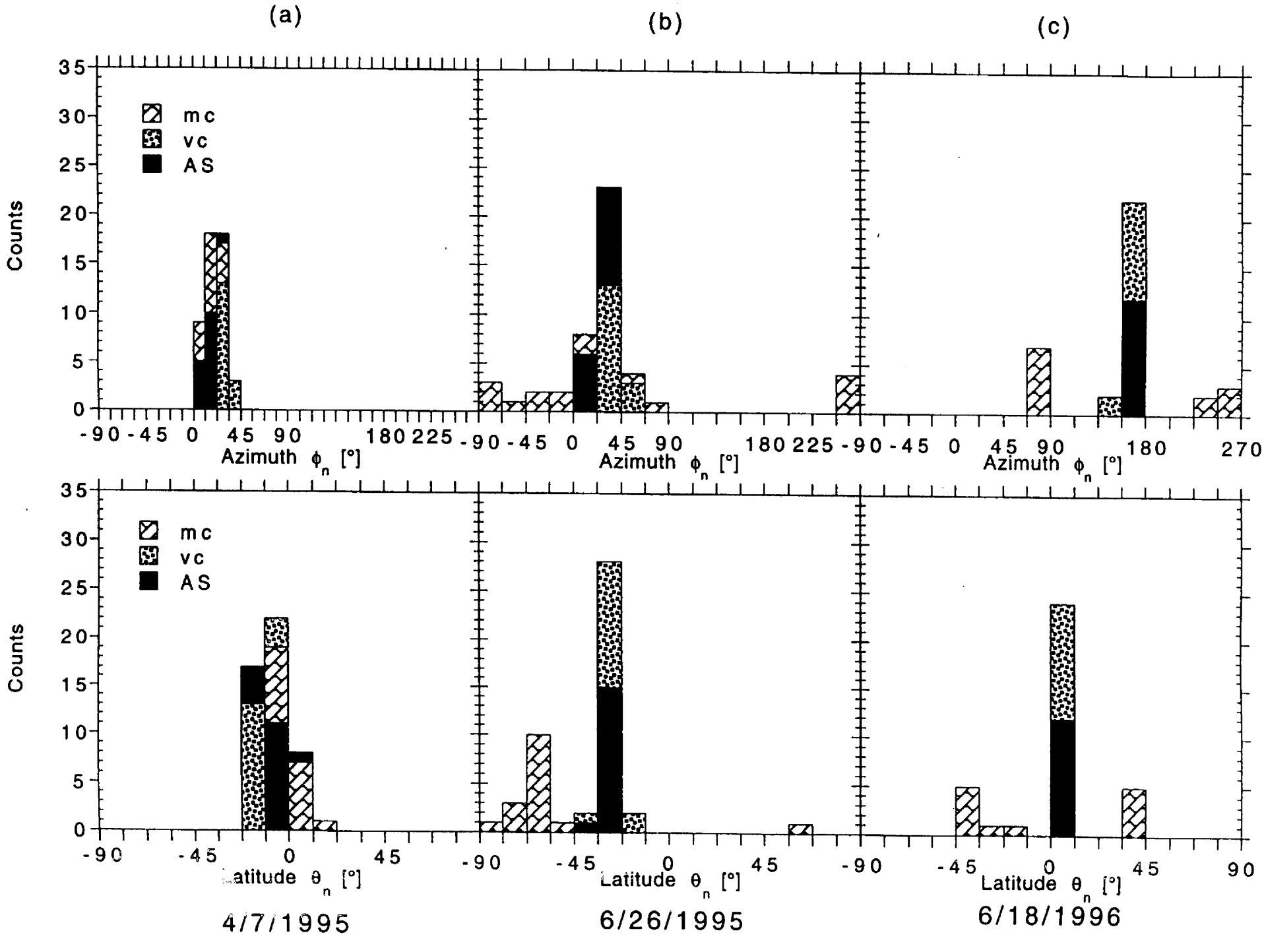
(a)
(b)
(c)
mc
vc
AS
Counts
Azimuth ϕ_n [°]
Latitude θ_n [°]
4/7/1995
6/26/1995
6/18/1996

Fig. 1

Fig. 2a

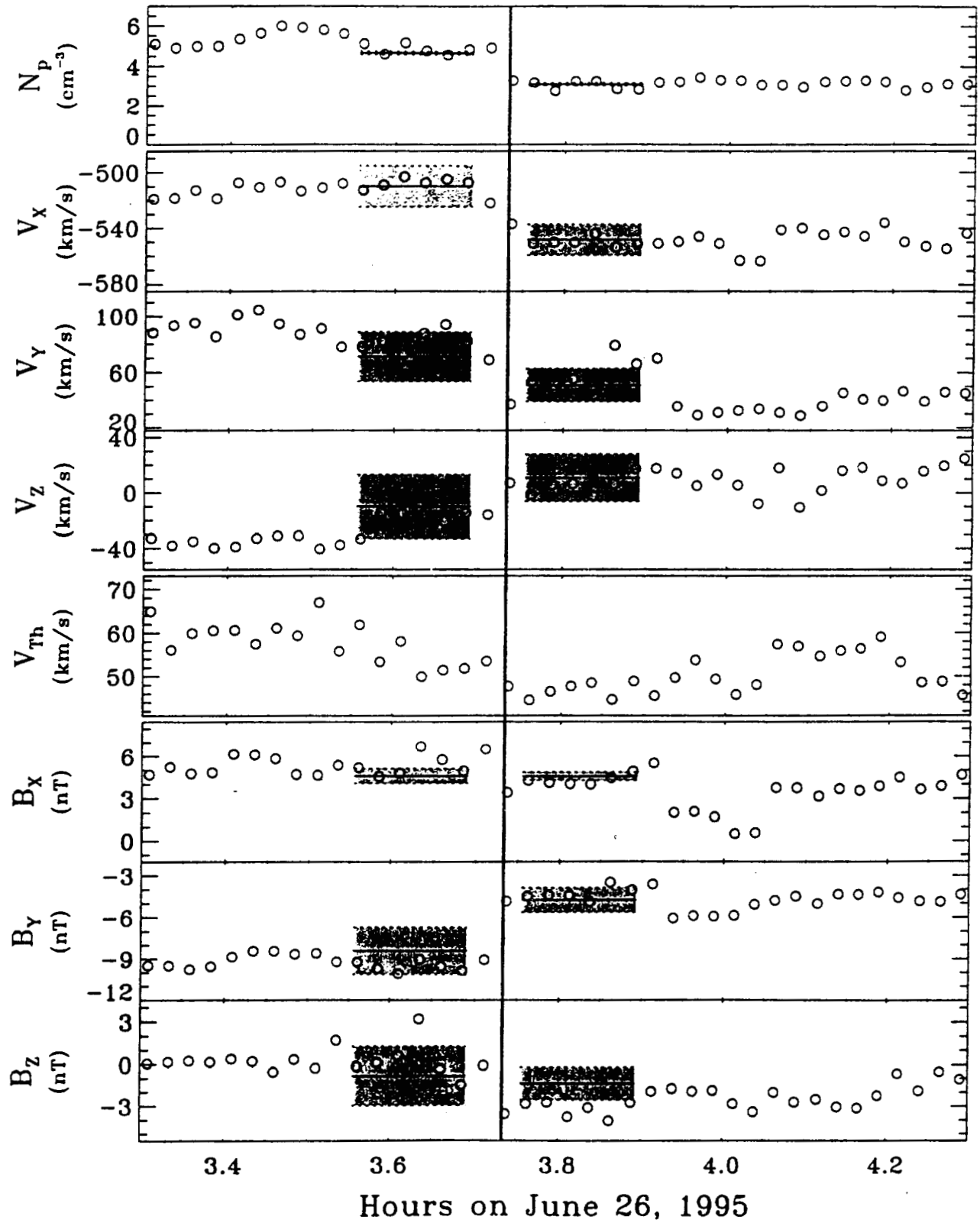
N_p (cm^{-3})
6
4
2
0
V_X (km/s)
−500
−540
−580
V_Y (km/s)
100
60
20
V_Z (km/s)
40
0
−40
V_{Th} (km/s)
70
60
50
B_X (nT)
6
3
0
B_Y (nT)
−3
−6
−9
−12
B_Z (nT)
3
0
−3
3.4
3.6
3.8
4.0
4.2
Hours on June 26, 1995

Fig. 2b

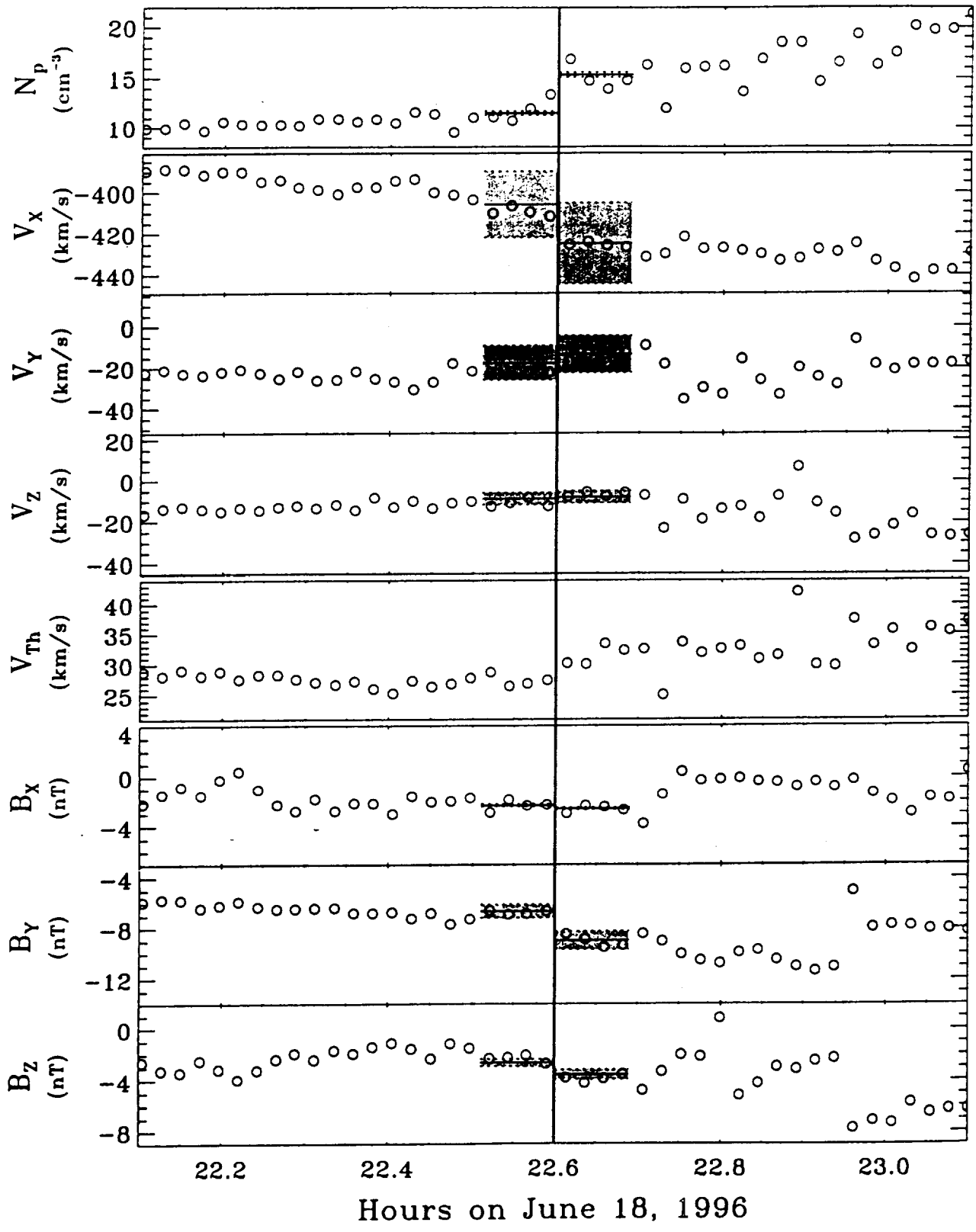
N_p (cm^{-3})
20
15
10
V_X (km/s)
−400
−420
−440
V_Y (km/s)
0
−20
−40
V_Z (km/s)
20
0
−20
−40
V_{Th} (km/s)
40
35
30
25
B_X (nT)
4
0
−4
B_Y (nT)
−4
−8
−12
B_Z (nT)
0
−4
−8
22.2
22.4
22.6
22.8
23.0
Hours on June 18, 1996

Fig. 3a

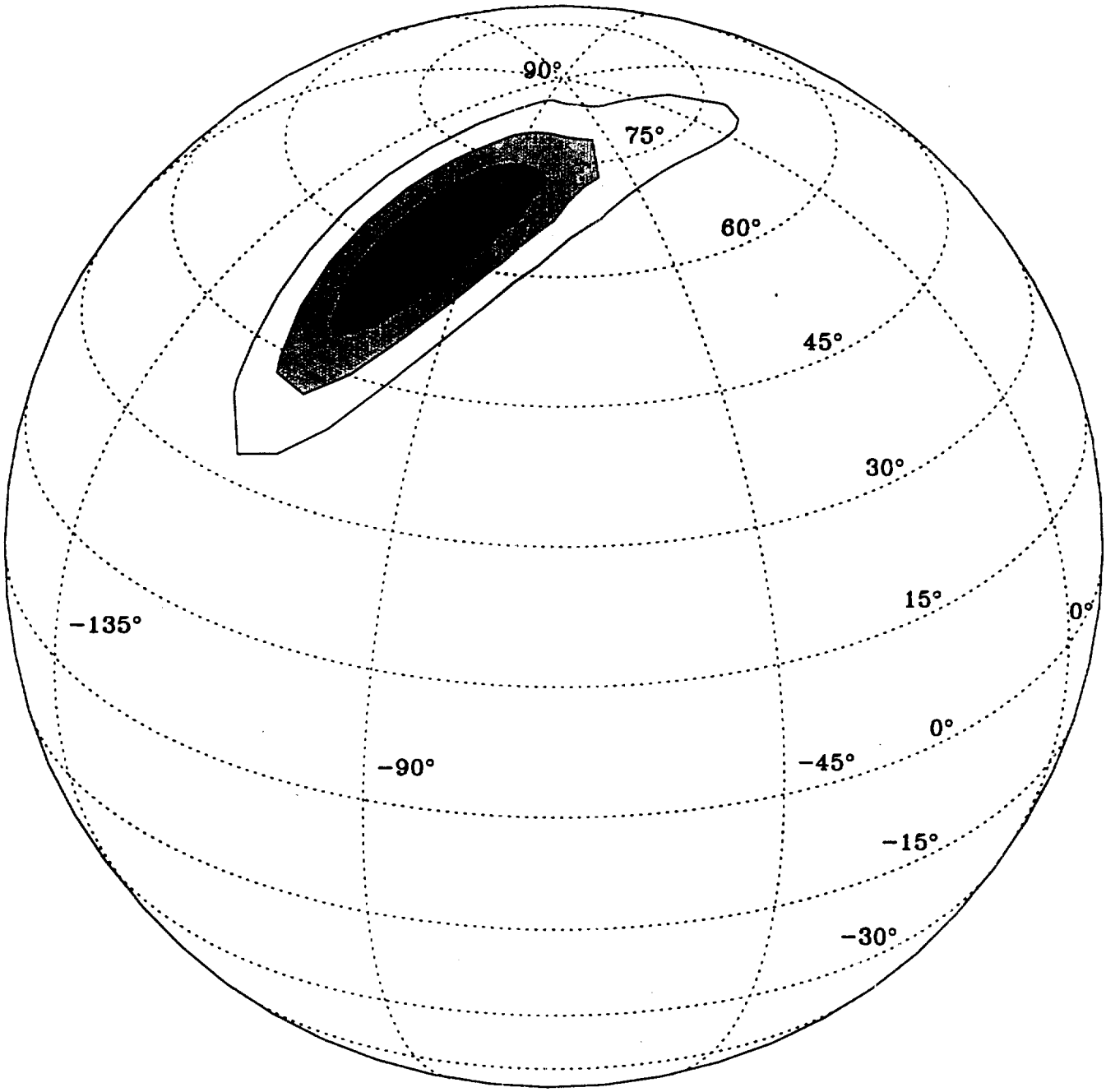

Fig. 36

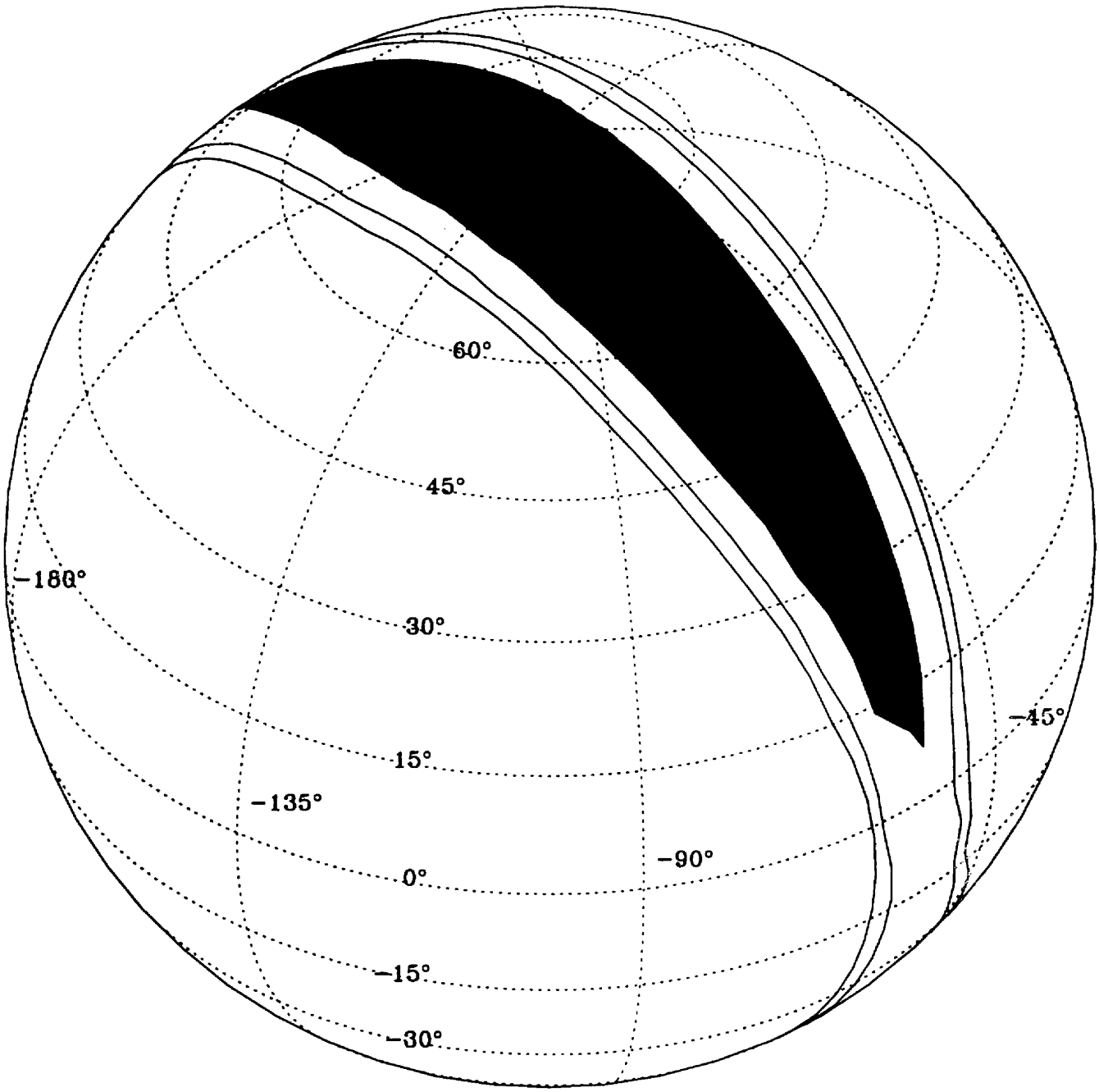

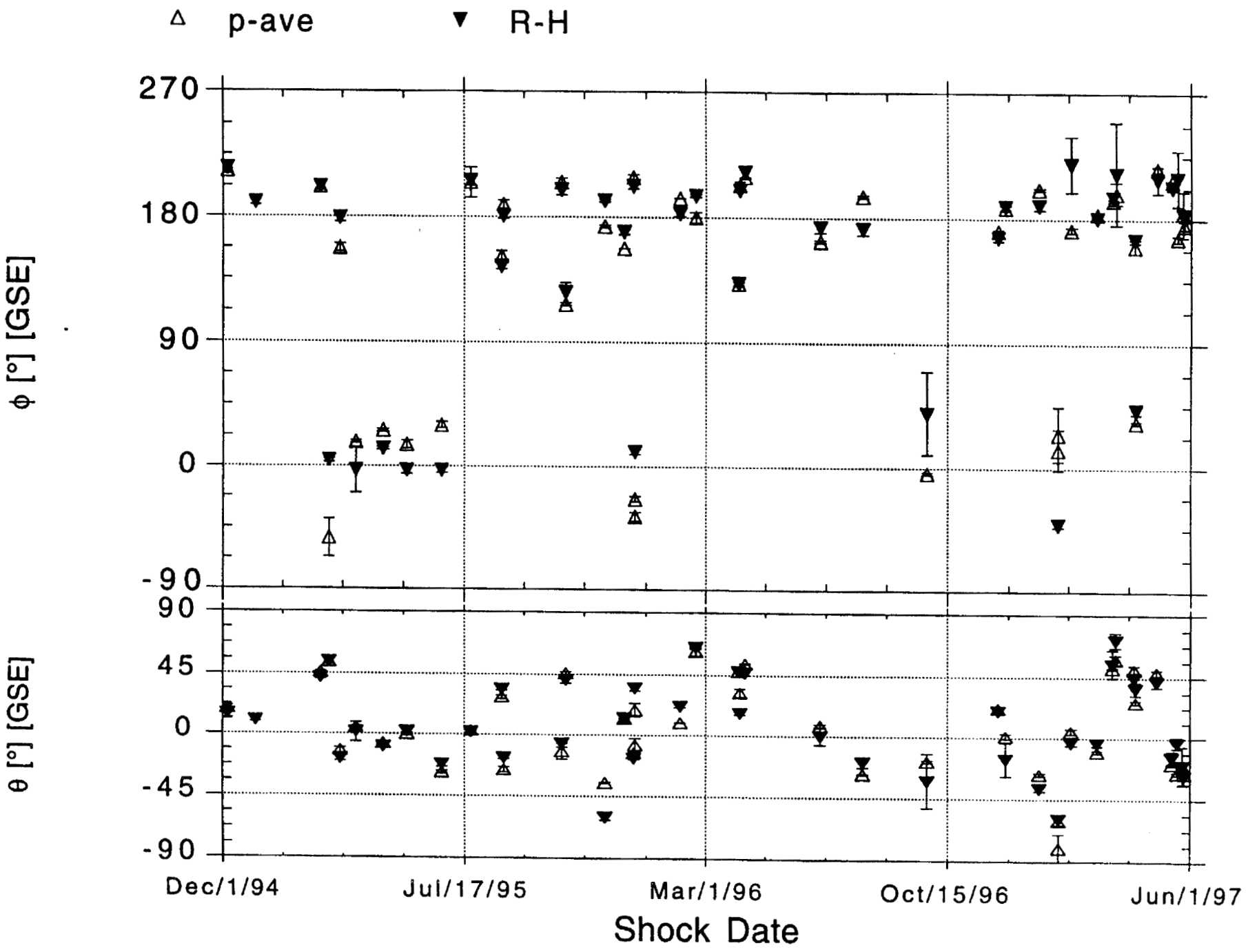
△ p-ave
▼ R-H
270
180
90
0
-90
φ [°] [GSE]
90
45
0
-45
-90
θ [°] [GSE]
Dec/1/94
Jul/17/95
Mar/1/96
Oct/15/96
Jun/1/97
Shock Date

Fig. 4

Fig. 5

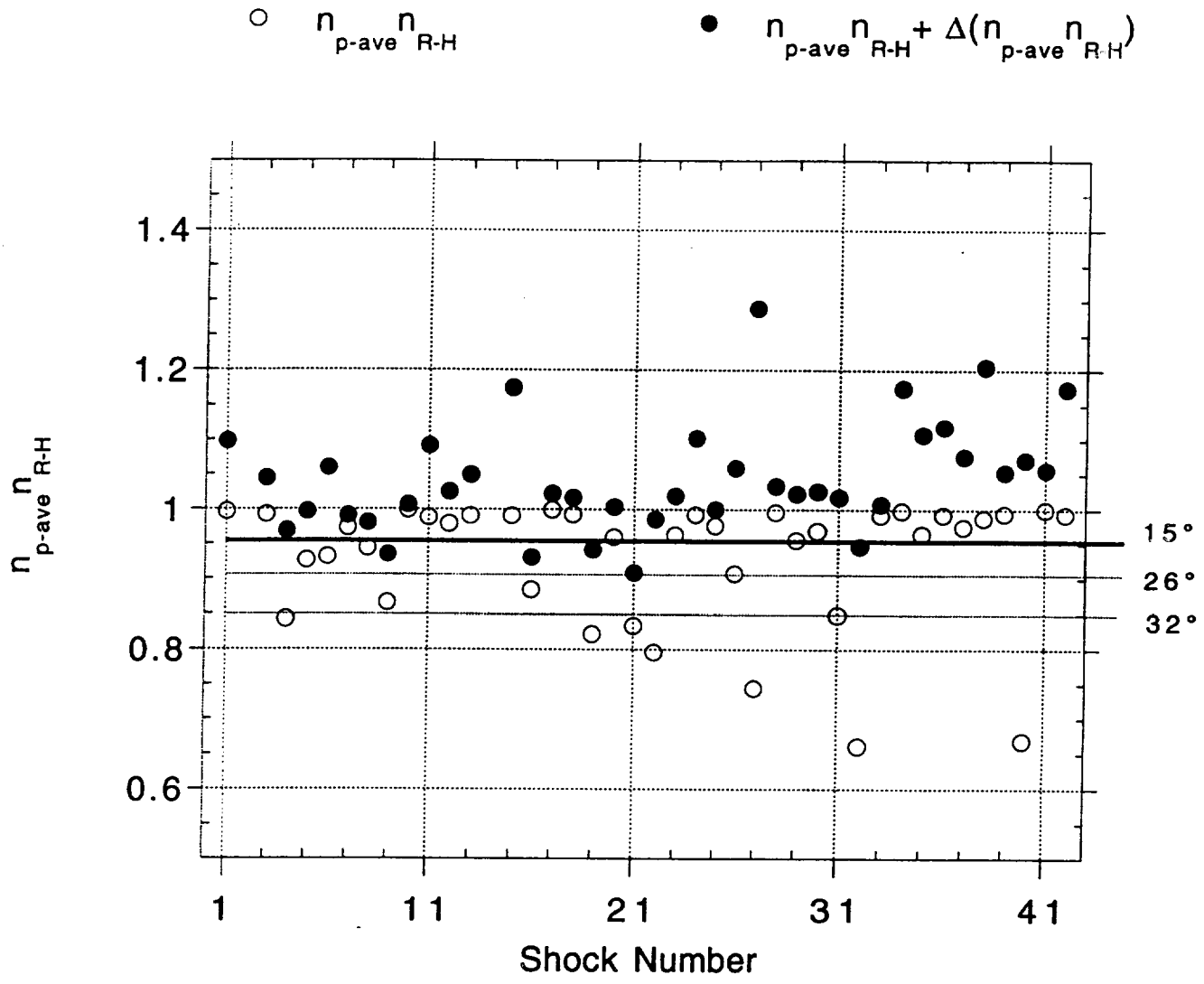
○ $n_{p\text{-}ave}n_{R\text{-}H}$
● $n_{p\text{-}ave}n_{R\text{-}H} + \Delta(n_{p\text{-}ave}n_{R\text{-}H})$
$n_{p\text{-}ave}n_{R\text{-}H}$
1.4
1.2
1
0.8
0.6
1
11
21
31
41
Shock Number
15°
26°
32°

Fig. 6

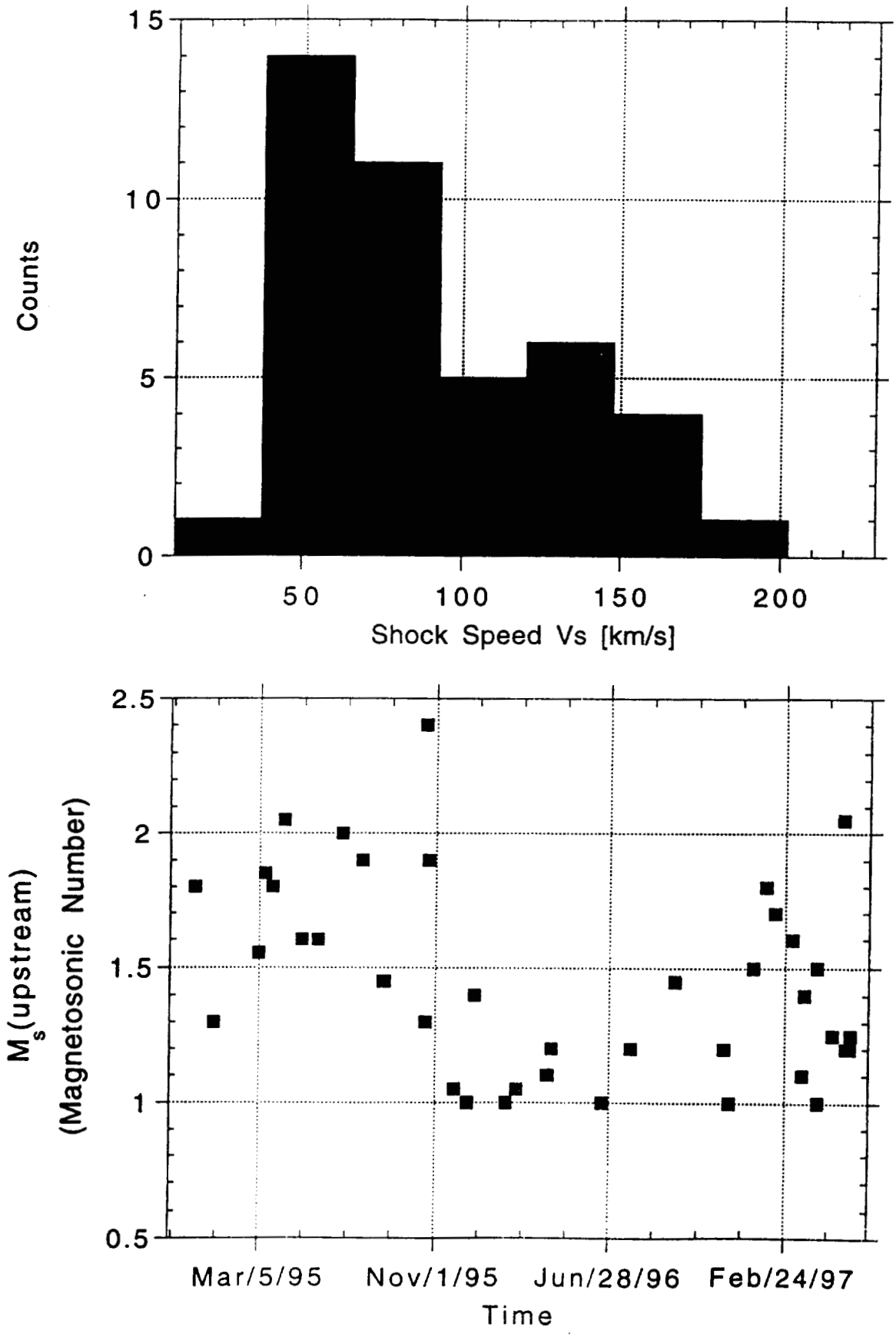
15
10
5
0
Counts
50
100
150
200
Shock Speed Vs [km/s]
2.5
2
1.5
1
0.5
M_s (upstream)
(Magnetosonic Number)
Mar/5/95
Nov/1/95
Jun/28/96
Feb/24/97
Time

Fig. 7

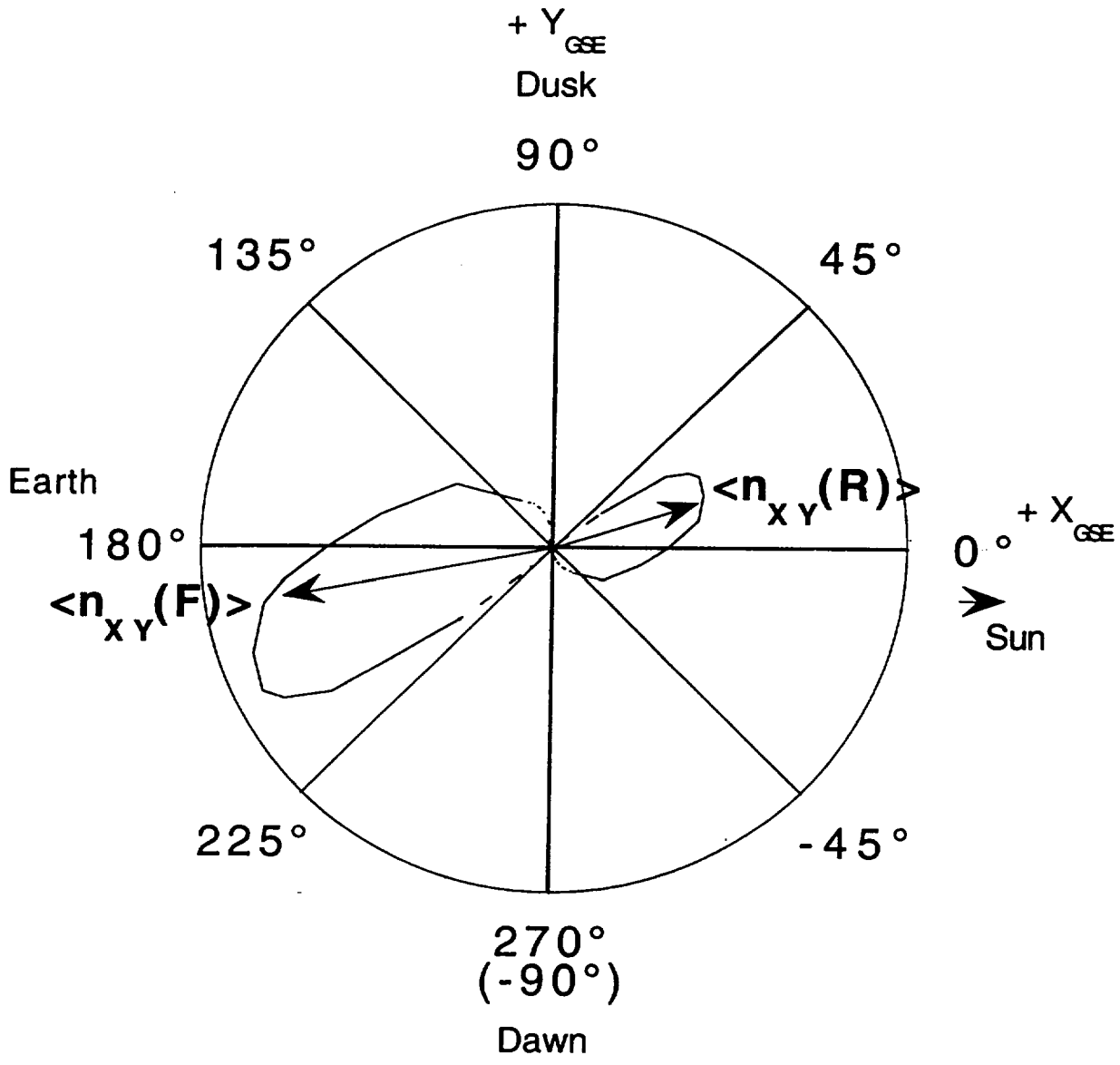
+ Y GSE
Dusk
90°
135°
45°
Earth
180°
<n X Y(F)>
<n X Y(R)>
0°
+ X GSE
Sun
225°
-45°
270°
(-90°)
Dawn

Fig. 8

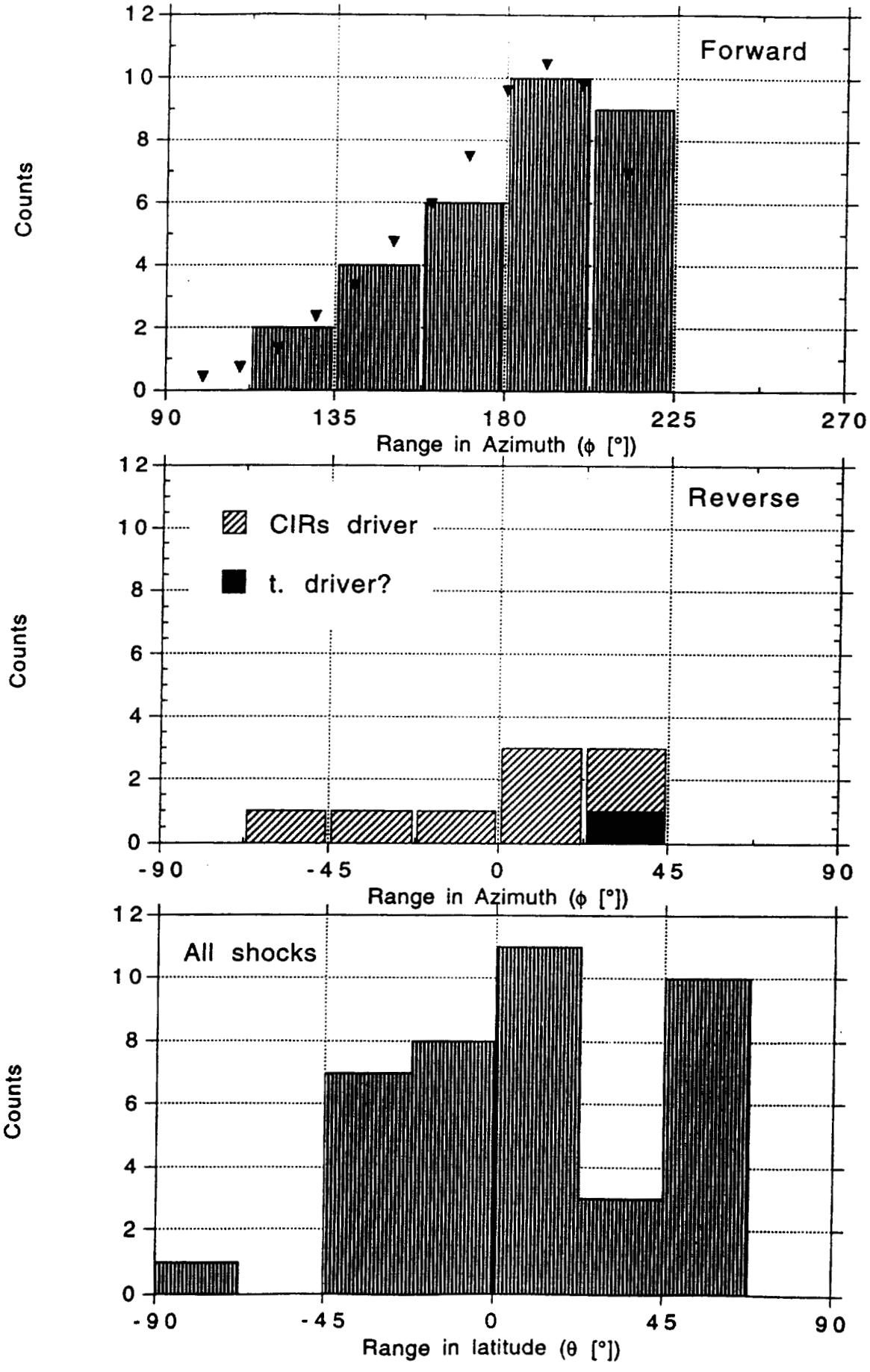
Forward
Counts
12
10
8
6
4
2
0
90
135
180
225
270
Range in Azimuth (ϕ [°])
Reverse
CIRs driver
t. driver?
Counts
12
10
8
6
4
2
0
-90
-45
0
45
90
Range in Azimuth (ϕ [°])
All shocks
Counts
12
10
8
6
4
2
0
-90
-45
0
45
90
Range in latitude (θ [°])

9 a

9 b

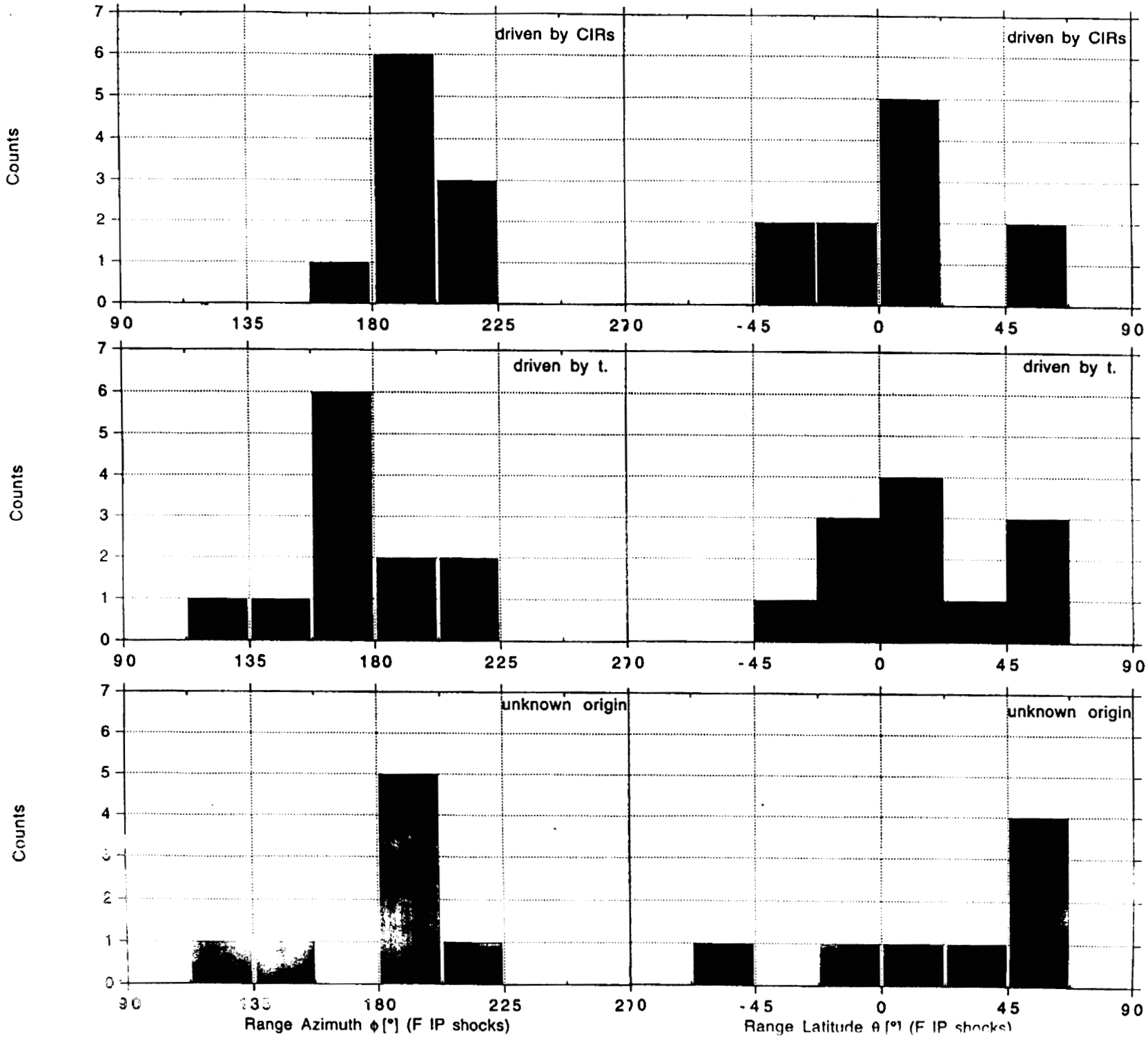
driven by CIRs
driven by CIRs
driven by t.
driven by t.
unknown origin
unknown origin
Counts
Counts
Counts
0
1
2
3
4
5
6
7
90
135
180
225
270
-45
0
45
90
Range Azimuth ϕ [°] (F IP shocks)
Range Latitude θ [°] (F IP shocks)

Fig. 9

Fig. 10

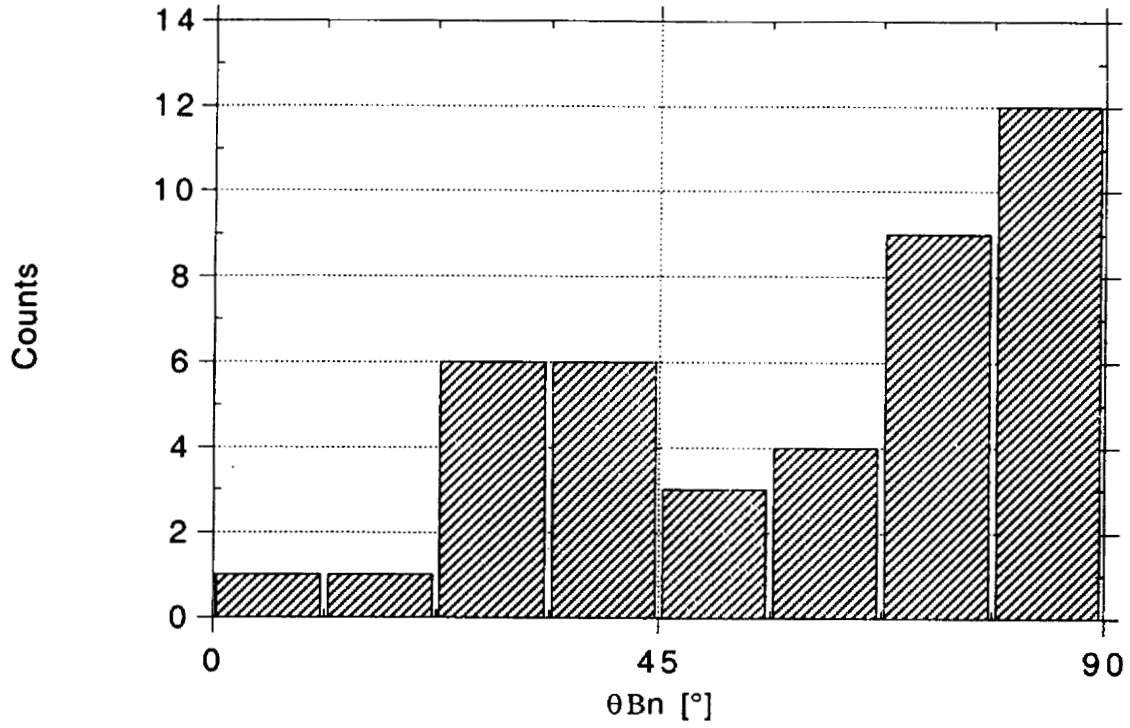

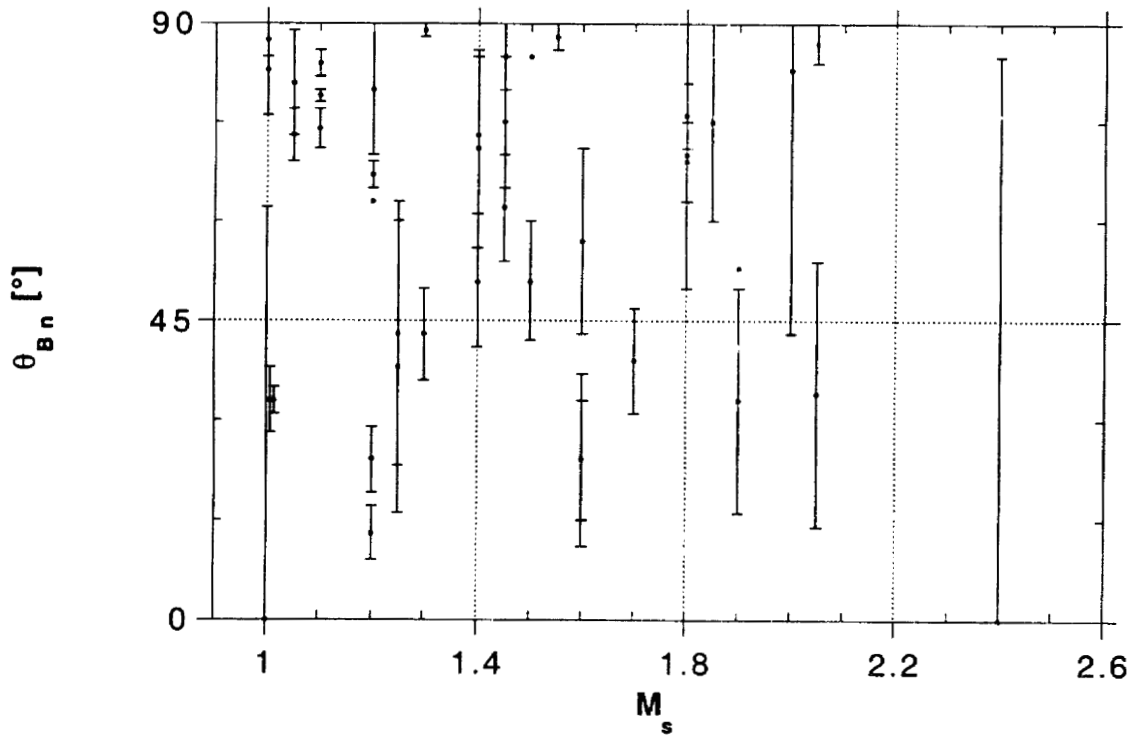

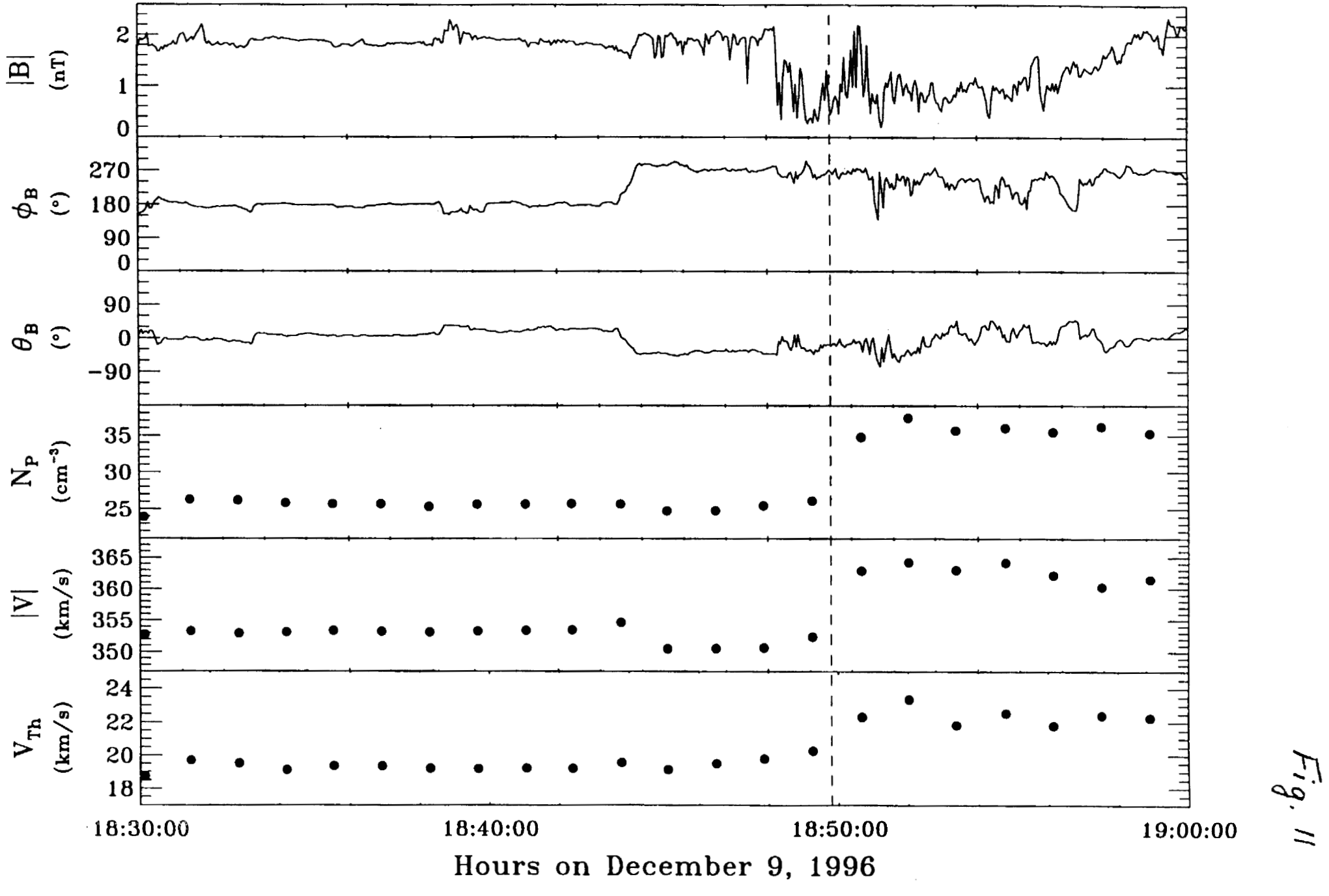
|B| (nT)
2
1
0
ϕ_B (°)
270
180
90
0
θ_B (°)
90
0
−90
N_P (cm^{-3})
35
30
25
|V| (km/s)
365
360
355
350
V_{Th} (km/s)
24
22
20
18
18:30:00
18:40:00
18:50:00
19:00:00
Hours on December 9, 1996

Fig. 11